scientific reports

Check for updates

OPEN

Bending performance of reinforced concrete beams with partial waste glass aggregate replacement assessed by experimental, theoretical and digital image correlation analyses

Yasin Onuralp Özkılıç[1,2]✉, Boğaçhan Başaran[3], Ceyhun Aksoylu[4], Memduh Karalar[5], Özer Zeybek[6], Essam Althaqafi[7], Alexey N. Beskopylny[8]✉, Sergey A. Stel'makh[9], Evgenii M. Shcherban'[10] & Osman Ahmed Umiye[1,11]✉

This study examines the usage of waste glass aggregate (WGA) for the consumption of sustainable reinforced concrete regarding the replacement of fine aggregate (FA) and coarse aggregate (CA). For this purpose, a series of tests consisting of a total of 12 beams were carried out to explore the bending performance. The quantity of the longitudinal reinforcement section area and WGA percentage were selected as the prime variables. For this purpose, the aggregate was swapped with WGA with weight percentages of 10% and 20% for the FA and 10% and 20% for coarse aggregate. The test outcomes revealed that the crack and bending properties of the reinforced concrete beams (RCBs) were greatly affected by the section area of tension reinforcement and the percentage of the WGA. The WGA percentage might be effectively used as 20% of the partial replacement of FA. With the addition of FA to the mixture, the load-bearing capacity of RCB increases. The increase in the WGA percentage by more than 10% might cause a considerable reduction in the capacity of the RCBs, especially when the longitudinal reinforcement ratio is high. Furthermore, the digital image correlation method was used to show the cracks/micro-cracks and to define displacement in RCBs.

Keywords Reinforced concrete, Beam, Waste glass powder, Recycled, Digital image correlation

Abbreviations

WGA	Waste Glass Aggregate
FA	Fine Aggregate
RCBs	Reinforced Concrete Beams
WG	Waste glass
c_i	The neutral axis depth

[1]Department of Civil Engineering, Faculty of Engineering, Necmettin Erbakan University, 42000 Konya, Turkey. [2]Department of Technical Sciences, Western Caspian University, Baku 1001, Azerbaijan. [3]Department of Construction, Vocational School of Technical Sciences, Amasya University, 05100 Amasya, Turkey. [4]Department of Civil Engineering, Faculty of Engineering and Natural Sciences, Konya Technical University, Konya 42250, Turkey. [5]Department of Civil Engineering, Faculty of Engineering, Zonguldak Bulent Ecevit University, 67100 Zonguldak, Turkey. [6]Department of Civil Engineering, Faculty of Engineering, Mugla Sitki Kocman University, 48000 Mugla, Turkey. [7]Civil Engineering Department, College of Engineering, King Khalid University, Abha 61421, Saudi Arabia. [8]Department of Transport Systems, Faculty of Roads and Transport Systems, Don State Technical University, Rostov-on-Don 344003, Russia. [9]Department of Unique Buildings and Constructions Engineering, Don State Technical University, Gagarin Sq. 1, Rostov-on-Don 344003, Russia. [10]Department of Engineering Geometry and Computer Graphics, Don State Technical University, 344003 Rostov-on-Don, Russia. [11]Department of Civil Engineering, Faculty of Engineering Technology, Zamzam University of Science and Technology, Mogadishu, Somalia. ✉email: yozkilic@erbakan.edu.tr; besk-an@yandex.ru; osmanomiye@zust.edu.so

ε_{ci}	The concrete compressive strain
d	The effective depth
ε_{si}'	The tensile reinforcement strain
ε_{si}	The compressive reinforcement strain
F_{si}'	The tensile reinforcement force (N)
F_{si}	The compressive reinforcement force (N)
F_{ci}	The concrete compressive force (N)
A_s	The tensile reinforcement area (mm^2)
A_s'	The compressive reinforcement area (mm^2)
f_{si}'	The tensile reinforcement stress (MPa)
f_{si}	The compressive reinforcement stress (MPa)
f_{cmi}	The concrete cylinder compressive strength (MPa)
k_i	The coefficient of equivalent rectangular concrete area
m	The distance from the neutral axis to the center of the concrete compressive force (mm)
M_{NAi}	The moment value of the beam section (Nmm)
P_{NAi}	The load bearing value of the beam (N)
a	The beam shear span (mm)
f_{cm}	The average cylinder concrete compressive strength (MPa)
E_c	The modulus of elasticity of concrete (MPa)
V_c	The shear strength obtained from concrete (N)
V_s	The shear strength obtained from transverse reinforcement (N)
V	The total shear strength (N)
f_c	Compressive strength (MPa) of the cylindrical concrete test samples
A_s	The area of the tensile reinforcement (mm^2)
b_w	The beam width (mm)
d	The effective depth of the beam (mm)
f_{yt}	The transverse reinforcement yield strength (MPa)
s	The distance between the transverse reinforcements (mm)
ρ	Tensile rebar ratio (A_s/b_w*d)
ρ'	Compressive rebar ratio (A_s'/b_w*d)

Concrete, which is frequently preferred in the construction industry, leads to a large consumption of raw materials and a high amount of CO_2 emissions. To overcome this problem, the production of environmentally friendly concrete is very important, which can reduce both CO_2 emissions and minimize the consumption of raw materials. Various types of waste materials are often preferred over cement and aggregate to reduce raw materials[1]. The use of different waste materials such as rubber, marble, tiles, and plastic instead of aggregate contributes to the production of sustainable construction materials[2,3].

Glass produced from raw materials such as sand is widely used in different industries. While a significant portion of discarded glass is recycled to manufacture new glass items, a considerable amount is still disposed of in landfills. One of the biggest problems with glass is that applications such as beverage bottles, which are one of the main usage areas of glass, are disposable. Global waste glass (WG) is estimated at 209 million tons per year, and failing to recycle glass constitutes a serious environmental danger[4]. One of the recycling methods for WG can be applied as the binder for the construction industry[5,6]. Another practical opportunity for consuming WG in cementitious resources is the replacement of coarse aggregate (CA) and fine aggregate (FA). Consumption of natural aggregates leads to the depletion of non-renewable resources, such as beaches and quarries, that cannot be replenished.

Harrison et al.[7] investigated the potential of including WG in cement-based materials. It was reported that WG is inappropriate as a raw material substitute for CA but it can be utilized as a replacement for FA. Batayneh et al.[8] examined the properties of concrete with ordinary Portland cement under the influence of consuming reused glass, plastic waste materials, and crushed concrete as a fraction of the aggregates. It was found that the strength of concrete combinations was enhanced because of the partial replacement of FAs with crushed glass aggregates, but the high alkali content of such aggregates would affect the long-term stability and strength, both of which need long-term examination. Tejaswi et al.[9] observed replacement of 20% FA via weight can generate comparable compressive strengths to the control, as replacement of 10%, 30%, 40%, and 50% generate lower compressive strength values. The study carried out by Khan and Sarker[10] tried to estimate the consumption of 25% to 100% WG as a replacement for natural aggregates such as sand on the possessions of alkali-activated mortars. Workability, compressive strength, drying shrinkage, penetrability, resistance to high-temperature experiences, and the microstructures of the alkali-activated mortars having FA obtained from WG were studied. Ahmad et al.[11] utilized recycled concrete aggregate for concrete mixture and WG to fill the voids of recycled concrete aggregate to mitigate negative performance effects. Dinh et al.[12] performed tensile and cracking tests on sustainable carbon-textile-reinforced cementitious composites made using expanded WG and fly ash as cement substitutes. AL-Bawi et al.[13] observed experimentally the influence of different amounts of green-colored WG cullet on the mechanical and rupture possessions of self-compacting concrete. For this aim, cullet was combined at different ratios (0%, 20%, 40%, 60%, 80%, and 100% by weight) as a replacement for natural FA and/or natural CA. It was found that the mechanical properties were negatively influenced by inclusion of WG cullet. An investigation into the characteristics of concrete using WG as FA was carried out by Arivalagan et al.[14]. WG was utilized for replacement of the sand at 10%, 20%, and 30%. This experiment showed that substituting WG powder with natural sand increased strength. Adaway and Wang[15] performed an experimental study to detect the properties of applying WG as a partial replacement for FA in structural-grade

concrete. For this aim, glass replacement proportions were chosen as 15, 20, 25, 30 and 40%. It was found that compressive strength was observed to rise to a level of 30%, at which point the strength advance was found as 9% and 6% greater than the control after 7 and 28 days respectively. This exhibits that concrete holding up to 30% fine glass aggregate demonstrates greater compressive strength improvement than traditional concrete. Topçu and Canbaz[16] investigated the applicability of the WG in concrete after the reusing procedures. For this purpose, tests were performed on the fresh and hardened concrete. It was found that the use of WG as aggregate had a minor impact on the fresh-state properties of concrete. Mohammed and Hama[17] observed the engineering properties of RCBs including 0% and 15% waste inclusion of glass aggregate (WGA) together with different amounts of plastic aggregate. For this aim, 15 beam samples with dimensions of 150 × 150 × 900 mm were prepared and tested. These samples were reinforced by altered longitudinal steel proportions of 2Ø8, 2Ø12, and 2Ø16 with two proportions of shear reinforcement. It was found that the beams with WG demonstrated a greater load-bearing capacity. Hama et al.[18] examined the influence of WG replacement with different cement weight proportions. Considering the load-deformation correlation, the beams with 10% WG have greater crack resistance ability than that of other beams. Mustafa et al.[19] investigated the flexural performance of RCBs having WG as a replacement for cement and FAs. The beams including 10% WG displayed an improvement in the ultimate load capacity. Hamid and Zubir[20] used WG to exchange the natural FA in different mix proportions for RCBs. Many different studies investigate the behavior of RCBs composing WG[21–24]. Legese et al.[25] investigated the characteristics of concrete utilizing waste glass and waste plastic as partial substitutes for fine aggregate. To determine the cement's compressive strength, splitting tensile strength, flexural strength, and workability, measurements were taken and analyzed. The ideal replacement of fine aggregate was determined to be 10%, with a ratio of 3% water-in-water and 7% water-in-water. This resulted in an increase in compressive strength of 12.55% and 6.44% at 7 and 28 days, respectively. Using waste glass powder as a partial cement replacement, Omer and Saeed[26] examined the behavior and flexural strength of reinforced concrete beams after 180 days. To achieve this objective, fourteen beams were evaluated, employing two GP particle sizes at substitution amounts between 0 and 15% for two different cement compositions. The test findings showed that, in contrast to the waste glass powder substitution level, the effect of waste glass powder particle size on the strength properties of beams was essentially insignificant. In another study, Safi et al.[27] investigated the assessment of concrete's compressive and flexural strengths using WG powder as a partial cement replacement. WG was substituted for cement in various amounts (0%, 10%, 15%, 17.5%, and 20%) in both cubic and prismatic specimens as part of the experimental study to address this. More strength was demonstrated by the 15% replacement than by the 10% replacement, while the 10% replacement was stronger than the 0% cement replacement. Significantly, on the 28th day, the 20% cement substitution showed negative over-strength percentages, including − 2.42% in compressive strength and − 1.42% in flexural strength. In addition, there are various studies in the literature regarding mixing ratios[24,28–34]. It is well acknowledged that the construction sector is a laggard in terms of the adoption of technology, mostly because of the nature of its operation. There are few studies on the challenges practitioners face in adopting smart technologies and strategies to promote their adoption, which can start the digital transformation of entire cities. Recent innovations in materials and technology aim to decrease the environmental impact of concrete construction, improve its durability and performance, and contribute to the sustainability of the built environment[35]. Yuan et al.[36] investigated the economic and environmental advantages of closed-loop recycling for various types of waste glass by techno-economic analysis and life-cycle evaluation, including transportation, crushing and separation, and waste usage phases. It was determined that for each ton of WG, 12.77 kW h electricity and 2.22 m^3 natural gas were used, and for packing glass, 15 kW h and 3.45 m^3. Furthermore, upon standardization, the overall environmental effect is reduced by 51% and 29%, respectively, via waste flat glass and waste packaging glass closed-loop. To increase sustainability, performance, and efficiency, the concrete building sector is investigating new technologies and methods.

Generally, previous research attempts show that WG can be applied as a substitute for natural sand. There is an absence in the experimental investigations of the RCBs including WG. For this purpose, a series of experiments have been carried out by the authors and presented in the literature. In these studies, the shear[37] and flexural[38] behaviors of reinforced concrete beams produced by using partial glass powder instead of conventional cement in concrete mixtures were investigated. In addition, the effects of partial glass aggregate substitution instead of conventional aggregate in concrete mixtures on the shear capacity of beams were investigated[39].

In this context, this study aims to investigate the bending performance of RCBs by replacing FAs and CAs with WG in certain proportions according to the shortcomings of the research. The beams including WG that were constructed from numerous WG mixes were subjected to flexural loading until they fail. The experimental results were then compared with the digital image correlation method. A total of twelve beams were constructed with similar reinforcement arrangements and support circumstances by making use of five different WG mixtures. These 12 beams were compared with 3 reference beams with the same conditions but without WG, tested in a previous study[38]. For this research, the parameters that are being investigated are the WG replacement rates of 10% and 20% by mass of the fine and coarse aggregates, respectively. The load-deflection curves from the experiment were analyzed and compared using the digital image correlation approach to explore ways to improve the exploitation of used WG as a sustainable construction material. Detailed analysis is given in the following sections.

Experimental procedure

In the study, Portland cement CEM I 32.5 was selected. The mixtures were designed to have a water/cement ratio of 0.50. In the mixture, 10% and 20% WG were used instead of FA, and CA. Figure 1 depicts the various sizes of WG employed in this investigation. The ratio between CA and FA was kept equal. The ratio of cement to aggregates was 20%. Increased use of WGA decreased the workability of concrete produced by including WGA.

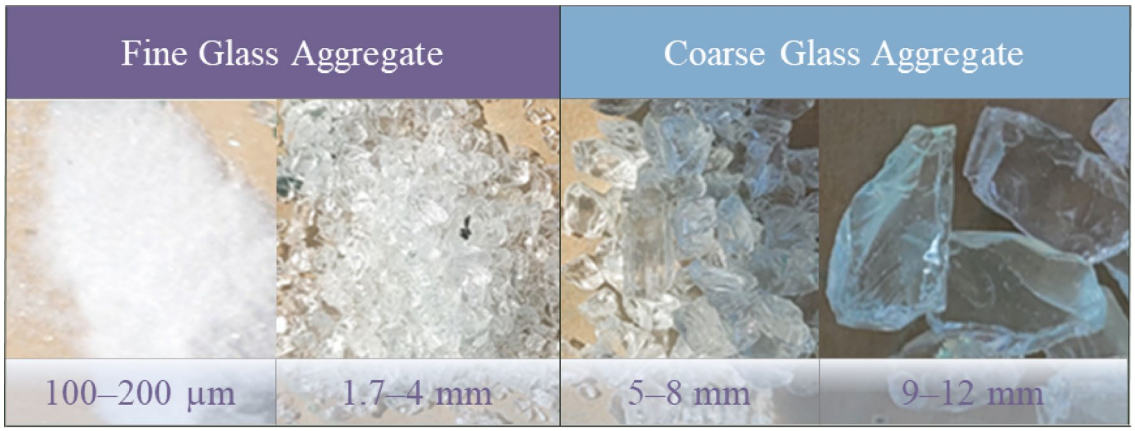

Fig. 1. Waste Glass Fine and Coarse Aggregate (WGA). (adapted from[39]).

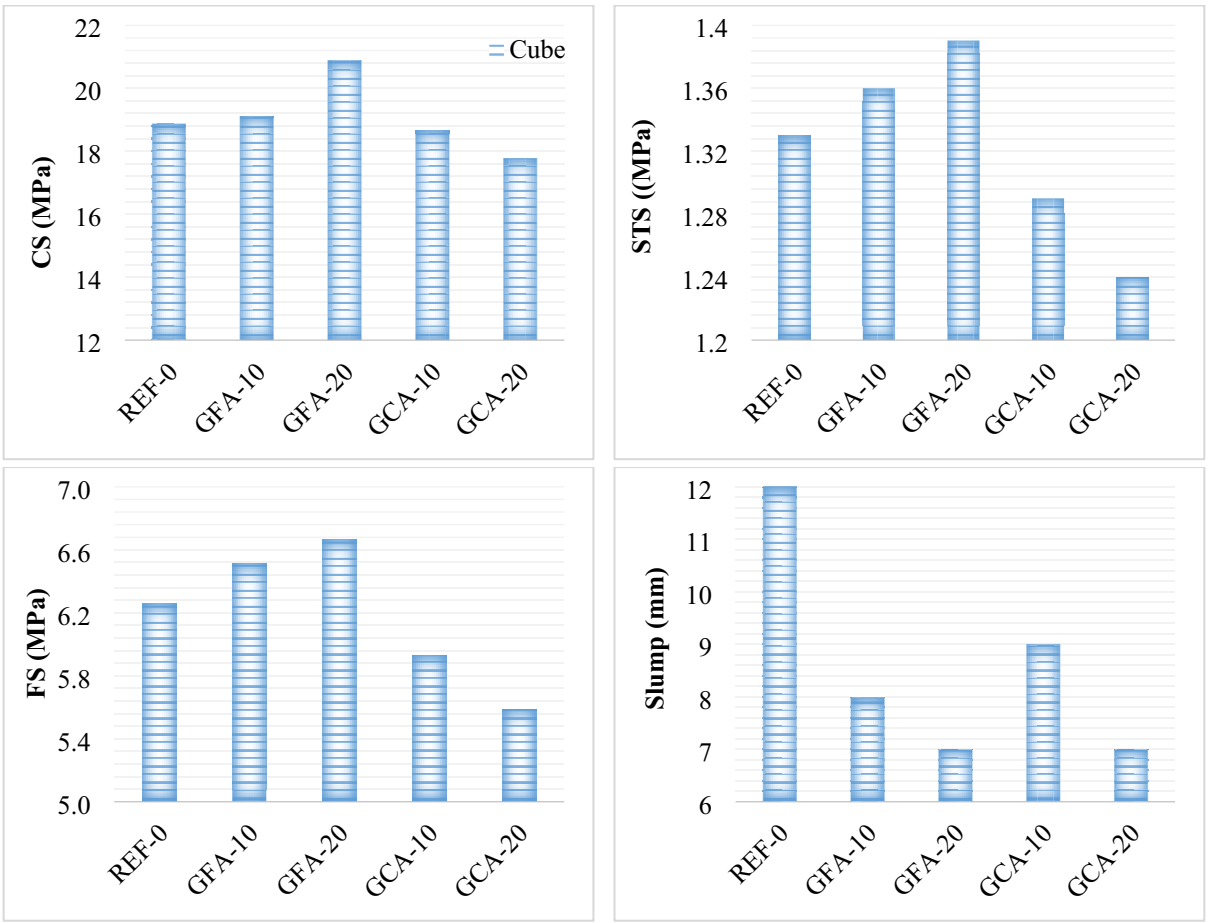

Fig. 2. Results of Concrete with fine and coarse aggregates. (adapted from[40]).

It employed CAs with a size range of 5–13 mm and FAs with a size range of 0–4 mm. Waste window glass was gathered from Akcihan Glass, Istanbul, Turkey, in the form of crushed and powdered waste glass. (soda lime glass). Fine glass trash consists of an equal quantity of glass measuring 1.7–4 mm and 100–200 microns. On the other hand, coarse glass waste consists of an equivalent amount of glass measuring 9–12 mm and 5–8 mm.

To assess the engineering properties of concrete containing discarded glass, three unique types of tests were conducted. Figure 2 demonstrates the mechanical findings of the specimens[40]. As the fine glass aggregate amounts increase, the capacities of the test specimens increase. On the other hand, the capacities decreased as the percentage of coarse glass aggregates increased. Workability decreased significantly after 20% fine aggregate

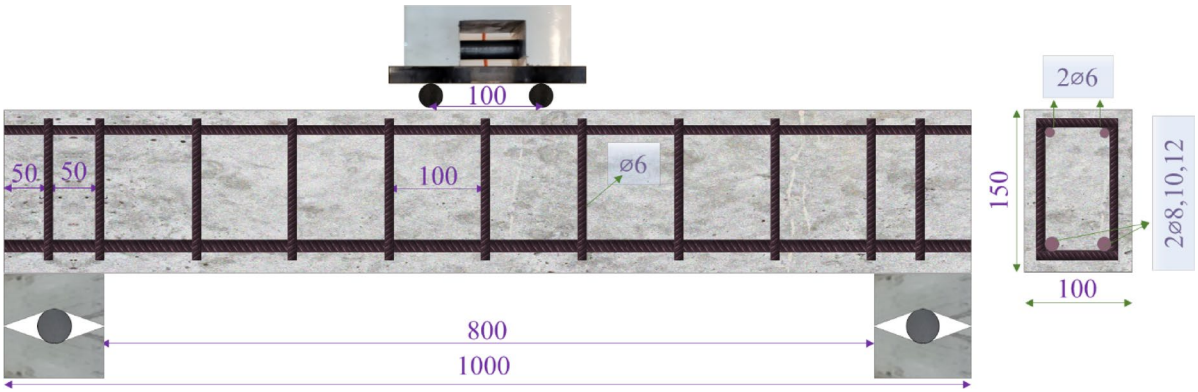

Fig. 3. Reinforcement Layout (in mm).

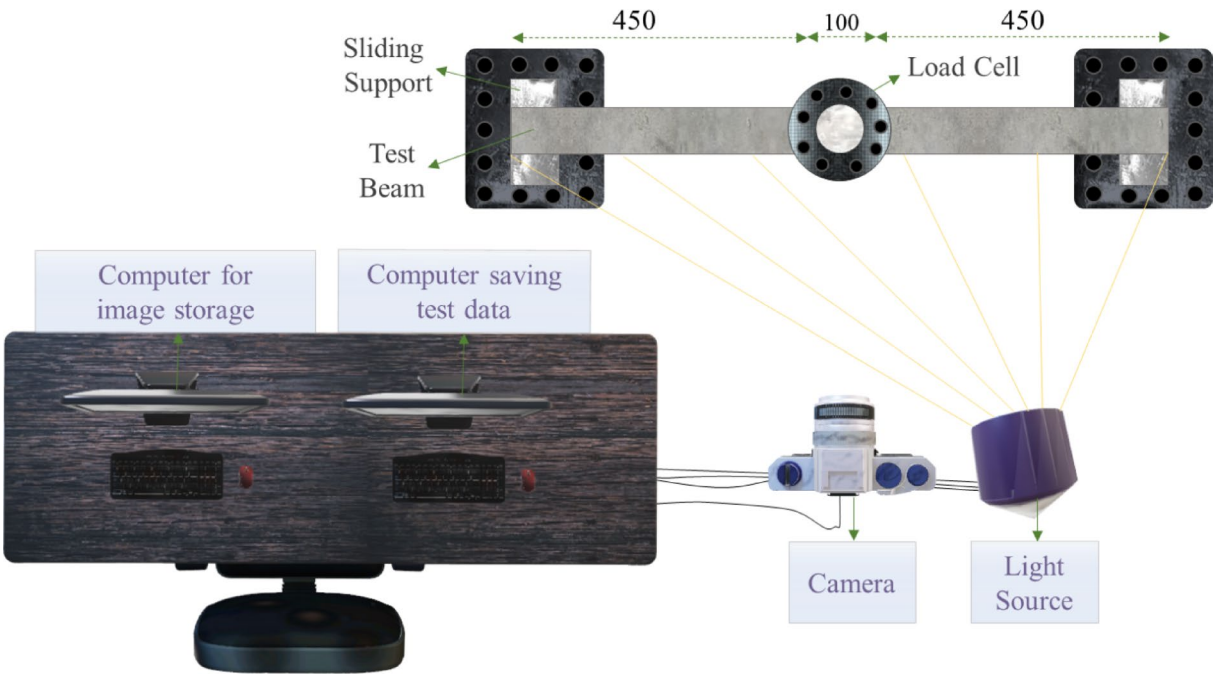

Fig. 4. Test Setup (in mm).

replacement[40]. Glass particles have sharper and more irregular geometric shapes than sand particles, causing increased friction and reduced fluidity[41]. The reason for this is that, instead of FA, glass fine aggregate (GFA), which does not absorb water at micro scales such as 100–200 microns, was used in the samples, which caused the pores in the concrete to decrease. Therefore, the compressive strength of the samples increased. However, this situation decreased the compressive strength of the concrete due to the increase in the brittleness of the glass aggregates in the samples where CA was replaced with glass coarse aggregate (GCA), despite the increase in diameters.

The beam tests were also conducted at the Civil Engineering Laboratory of Necmettin Erbakan University, where the specimens were also created. There were 15 distinct beams manufactured in all. The dimensions of the specimens were determined to be 100 × 150 × 1000 mm. To accomplish a bending behavior, Ø6/100 mm stirrups and a shear span-to-effective depth of 2.69 were selected as suitable specifications. Figures 3 and 4 show both the reinforcing scheme and the test setup, respectively.

Three of these samples were utilized as references and had no WGA, whereas the remaining samples contained 10% and 20% WGA, according to the weight (w_f) ratios of the specimens. The features obtained from the test samples are offered in Table 1.

No	Name	Replacement			Reinforcement				
		Aggregate Type	Ratio (%)	Tensile	ρ (%)	Compression	ρ' (%)	ρ-ρ' (%)	Transverse
1	B-GR1_0% [38]	-	0	2Ø12	1.74	2Ø6	0.43	1.30	Ø6/100
2	B-GR2_0% [38]	-	0	2Ø10	1.21	2Ø6	0.43	0.77	Ø6/100
3	B-GR3_0% [38]	-	0	2Ø8	0.77	2Ø6	0.43	0.34	Ø6/100
4	B-GCA1_10%	CA	10	2Ø12	1.74	2Ø6	0.43	1.30	Ø6/100
5	B-GCA2_10%	CA	10	2Ø10	1.21	2Ø6	0.43	0.77	Ø6/100
6	B-GCA3_10%	CA	10	2Ø8	0.77	2Ø6	0.43	0.34	Ø6/100
7	B-GCA4_20%	CA	20	2Ø12	1.74	2Ø6	0.43	1.30	Ø6/100
8	B-GCA5_20%	CA	20	2Ø10	1.21	2Ø6	0.43	0.77	Ø6/100
9	B-GCA6_20%	CA	20	2Ø8	0.77	2Ø6	0.43	0.34	Ø6/100
10	B-GFA1_10%	FA	10	2Ø12	1.74	2Ø6	0.43	1.30	Ø6/100
11	B-GFA2_10%	FA	10	2Ø10	1.21	2Ø6	0.43	0.77	Ø6/100
12	B-GFA3_10%	FA	10	2Ø8	0.77	2Ø6	0.43	0.34	Ø6/100
13	B-GFA4_20%	FA	20	2Ø12	1.74	2Ø6	0.43	1.30	Ø6/100
14	B-GFA5_20%	FA	20	2Ø10	1.21	2Ø6	0.43	0.77	Ø6/100
15	B-GFA6_20%	FA	20	2Ø8	0.77	2Ø6	0.43	0.34	Ø6/100

Table 1. Characteristics of the test samples (in mm). * (0%, 10%, 20%: Weight% of WGA).

Experimental results and discussion

The shear performances of RCBs with WGA were previously investigated by the authors[39]. In this part of the investigation which is the continuation of the previous work[39], bending RCBs are investigated in detail. For this purpose, bending RCBs were designed, and the results were evaluated.

Influence of longitudinal reinforcement amount on the performance of concrete produced with WGA

The reference RCB samples are represented using B-GR and the WGA-added RCBs are reflected using B-GCA and B-GFA. As mentioned above, FA symbolizes fine aggregates replacement and CA symbolizes coarse aggregates replacement. For example, B-GR1_0% represents an RCB with a WGA including 0%. Correspondingly, B-GCA_20% represents an RCB via a WGA including 20%. The details of the obtained results are given in the following sub-sections.

Situation 1: fracture and load-carrying performance of RCB (B-GR1_0%, B-GR2_0%, B-GR3_0%)

In this section, in order to compare the beams with glass aggregate reinforced concrete with beams with unreinforced concrete, the reference beams in the literature, which have been previously performed by the authors, are re-presented and interpreted[38]. Beams with different flexural reinforcements were produced without WGA admixture and tested under vertical load. As shown in Fig. 5, the load-bearing capacity of the RCBs was determined from the load-displacement curves. Furthermore, the damaged regions and the final failure mode on the beam were observed. As depicted in Fig. 5, In the beam with Ø12 longitudinal reinforcement, the maximum load point was identified as 50.85 kN, and the ultimate displacement was observed to be 23.45 mm. For the beam with Ø10 longitudinally employed, the above-mentioned values became 46.72 kN and 24.83 mm. On the other hand, when the beam with Ø8 longitudinally was utilized, it was realized that the above-mentioned values decreased to 39.32 kN and 52.75 mm. These results indicate that changes in the longitudinal reinforcement diameter have a significant impact on the load-bearing capacity and displacement behavior of the beams. Specifically, as the diameter of the longitudinal reinforcement in the tensile regions of the beams decreases, a reduction in the load-bearing capacity is observed, while the vertical displacement capacity increases. Additionally, a reduction in the longitudinal reinforcement diameter is associated with an increase in bending damage as opposed to shear damage in the beams. Consequently, the beams exhibit ductile behavior, leading to failure modes characterized by bending rather than shear. The failure mode of the samples after carrying out the tests is depicted in Fig. 5.

Situation 2: load-bending and fracture behavior of RCB (B-GCA1_10%, B-GCA2_10%, B-GCA3_10%)

In this part of the investigation, WGA in the test samples is selected as 10% with different longitudinal reinforcement amounts i.e. Ø12, Ø10, and Ø8. Impact of strengthened longitudinally amount on the fracture and failure patterns of the test samples was examined. As depicted in Fig. 6, changes in the load-deformation of the test samples were identified and the fracture and failure behavior of the test samples were noticed. As noticed in Fig. 6, when the Ø12 reinforced longitudinally selected was used, the load carrying capacity was equal to 52.63 kN, and the ultimate deformation was observed as 13.55 mm. If the Ø10 reinforced longitudinally was employed, the values mentioned above were detected as 46.34 kN and 20.46 mm. If the Ø8 reinforced longitudinally was utilized, the values mentioned above reached 37.82 kN and 49.68 mm. According to the load-deformation behavior shown in Fig. 6, the load-bearing capacity of the test samples increases as the WGA

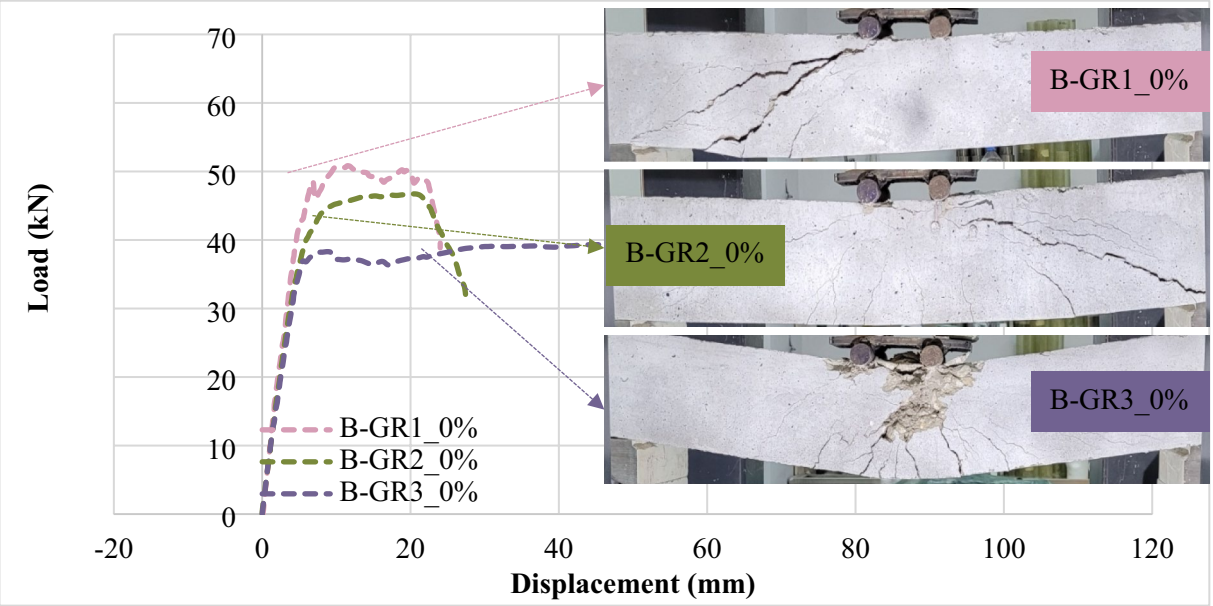

Fig. 5. Load-displacement and failure statement of test examples for B-GR1_0%, B-GR2_0%, B-GR3_0%[38].

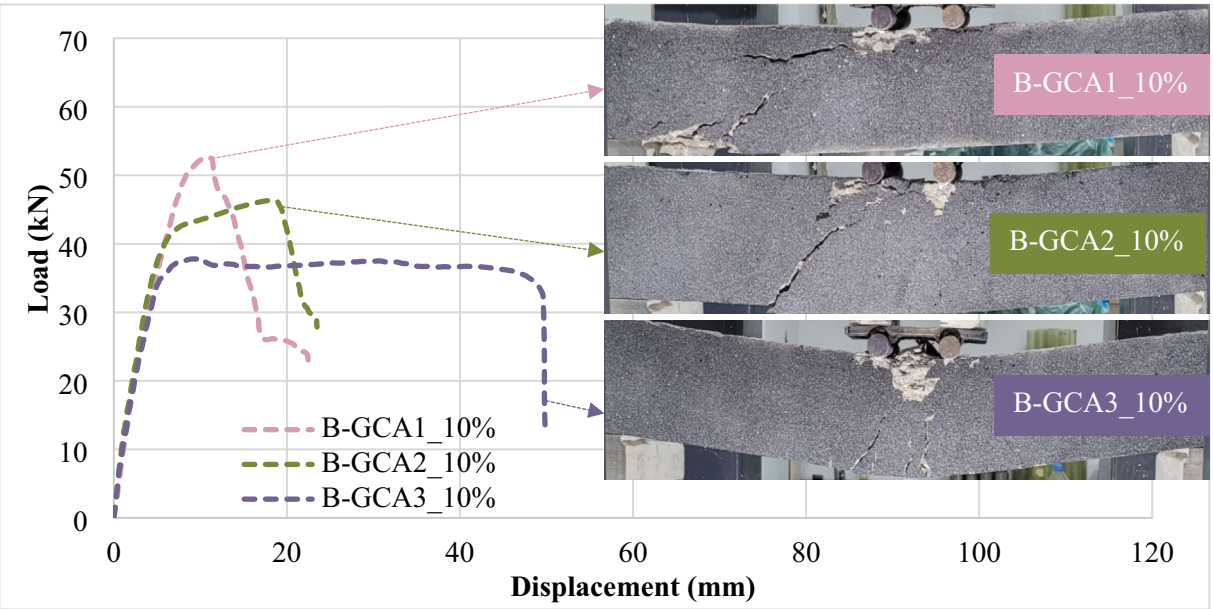

Fig. 6. Load-displacement and failure statement of test examples for B-GCA1_10%, B-GCA2_10%, B-GCA3_10%.

percentage rises. This enlargement changes with reference examples with no WGA. According to the beam with Ø12 tensile reinforcements, by considering two tensile reinforcements such as Ø10 and Ø8, the percentage of reduction was observed as 11.9% and 28.1%, respectively. Additionally, as the WGA percentage increased from 0% to 10%, no significant change was observed in the load-carrying capacity of the test samples. To put it another way, characteristic shear bending subject to ductility was noticed in B-GCA1_10% and B-GCA2_10% examples, as B-GCA3_10% example provides adequate ductility up to the maximum load, then it is subjected to bending deformation and distorted.

Situation 3: load-bending and fracture behavior of RCB (B-GCA4_20%, B-GCA5_20%, B-GCA6_20%)
WGA in the test samples is selected as 20% with different strengthened longitudinally amounts i.e. Ø12, Ø10, and Ø8. As presented in Fig. 7, the load-deformation behavior of the specimens was determined, and the fracture and failure patterns of the test specimens were noticed. As depicted in Fig. 7, when the Ø12 reinforced longitudinally

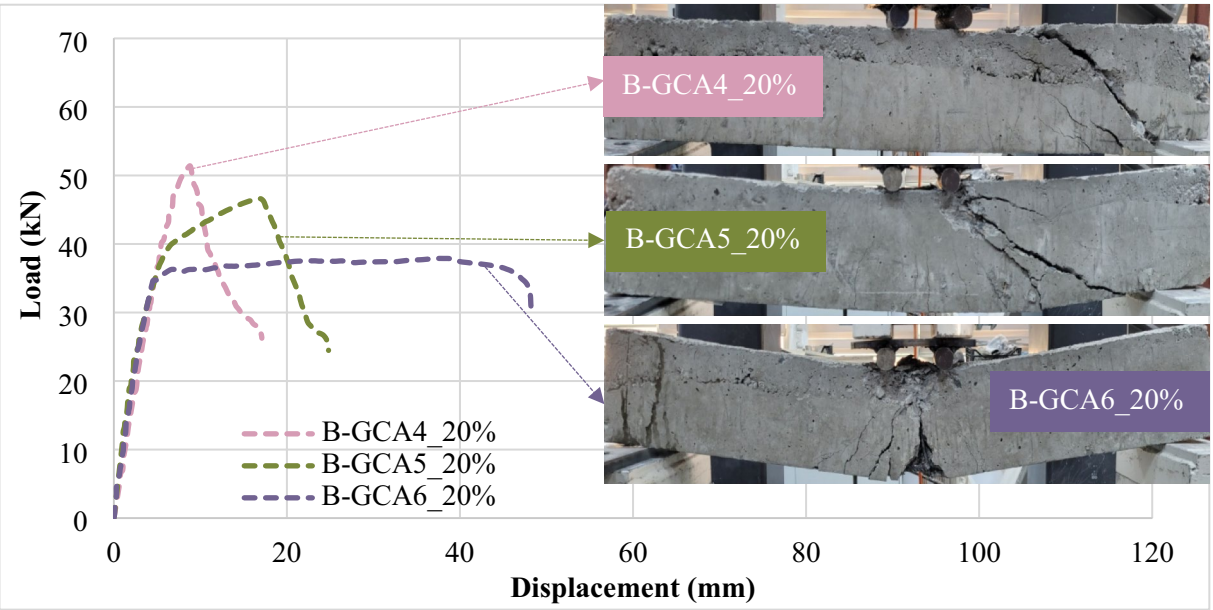

Fig. 7. Load-displacement and failure statement of test examples for B-GCA4_20%, B-GCA5_20%, B-GCA6_20%.

is used, the maximum load carrying capacity was 51.40 kN, and the ultimate deformation reached 10.28 mm. On the other hand, if the Ø10 and Ø8 reinforced longitudinally were considered, the above-mentioned values were 46.60 kN and 19.43 mm, and 37.89 kN and 48.14 mm, respectively. According to the load-displacement relationship given in Fig. 7, the load-bearing capability of the specimen improved as the reinforced longitudinally diameter enhanced from Ø8 to Ø12. To put it another way, the rupture pattern altered from flexural crack to shear crack type. Characteristic shear failure exposed to ductility was noticed in B-GCA4_20% and B-GCA5_20% samples, as B-GCA6_20% samples provided reasonable ductility until the maximum load, after this load it was subjected to bending and failure occurred. The results showed that as the diameter of the tensile reinforcement diminished from Ø12 to Ø8 (for 20% WGA percentage), load-displacement capability changed by −9.3% and −26.3% over the reference sample.

Situation 4: load-bending and fracture behavior of RCB (B-GFA1_10%, B-GFA2_10%, B-GFA3_10%)
In this part of the investigation, WGA replacing FA in the RCB is selected as 10%. Ø12, Ø10, and Ø8 longitudinal reinforcements are used to study the effect of the longitudinal reinforcement amount on the fracture and failure patterns of the test specimens. For this goal, reinforced longitudinally amounts were designated by taking Ø12, Ø10, and Ø8 into account. In the specimens, WGA was replaced with 10% FA. The load-deformation curves of the test specimens were obtained, and the fracture and failure patterns of the test samples were identified. As depicted in Fig. 8, when the Ø12 reinforced longitudinally was used, the maximum load bearing capacity and ultimate displacement were 57.10 kN and 16.39 mm, respectively. On the other hand, if the Ø10 and Ø8 reinforced longitudinally were utilized, these values became 46.03 kN-38.81 mm and 40.89 kN-41.19 mm, respectively. As mentioned above earlier, the load-bearing capability of the test sample enhancement as the reinforced longitudinally diameter improved from Ø8 to Ø12. In addition, when FA is used instead of coarse aggregate, it has been noticed that load-carrying capacity of the reinforced concrete beam increases significantly.

Situation 5: load-bending and fracture behavior of RCB (B-GFA4_20%, B-GFA5_20%, B-GFA6_20%)
In this part of the investigation, WGA replacing FA in the test specimen is selected as 20% as strengthened longitudinally quantities are designated as Ø12, Ø10, and Ø8 to study the effect of different reinforced longitudinally amount on the fracture and failure patterns of the test specimens. The load-displacement curves of the RCB are presented in Fig. 9, and the fracture and failure patterns of the samples are observed. As depicted in Fig. 9, when the Ø12 reinforced longitudinally was used, the maximum load carrying capacity and ultimate displacement were 61.37 kN and 21.34 mm. On the other hand, if the Ø10 and Ø8 reinforced longitudinally were utilized, the values above mentioned became 53.75 kN-44.94 mm and 41.72 kN-35.81 mm, respectively. As stated previously, the load-bearing capability of the sample improved as the reinforced longitudinally diameter enhanced from Ø8 to Ø12. In addition, while GFA is chosen instead of coarse glass aggregate a substantial increase in the load-carrying capacity of the reinforcement concrete beam was observed. This change became 19.4%, 15.3% and 10.1 for Ø12, Ø10 and Ø8.

Effect of WGA amount on the RCB

In this section, to explore the influence of different WGA proportions on reinforcement concrete, RCBs were considered as different WGA percentages. For this purpose, the weight percentages of 0%, 10%, 20% CA

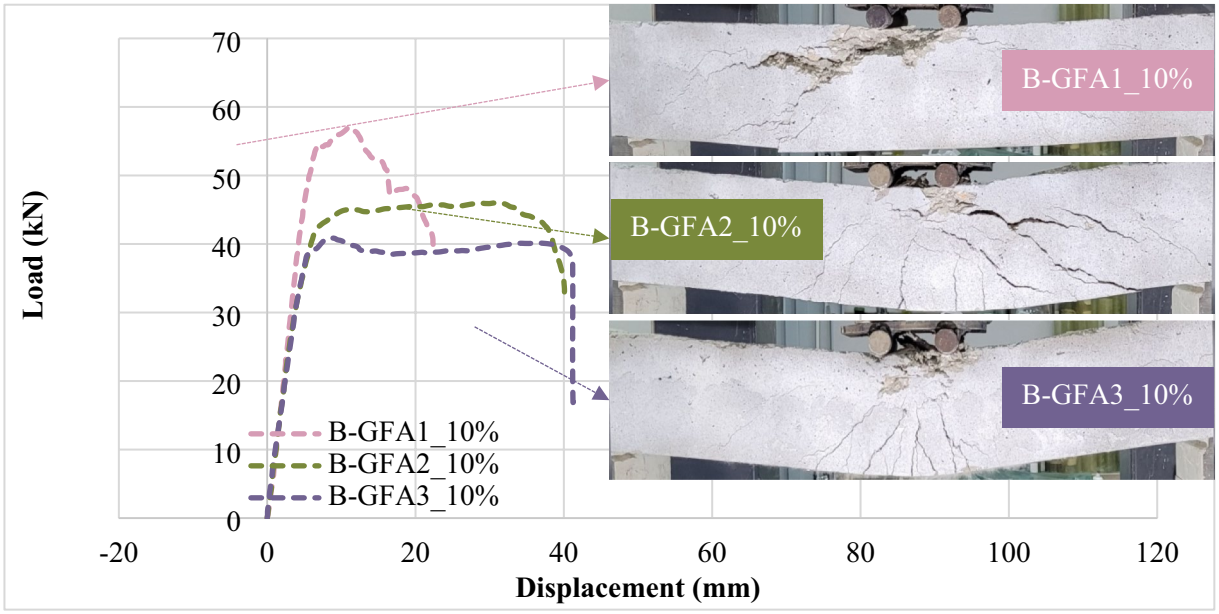

Fig. 8. Load- deformation, and failure statement of test examples for B-GFA1_10%, B-GFA2_10%, B-GFA3_10%.

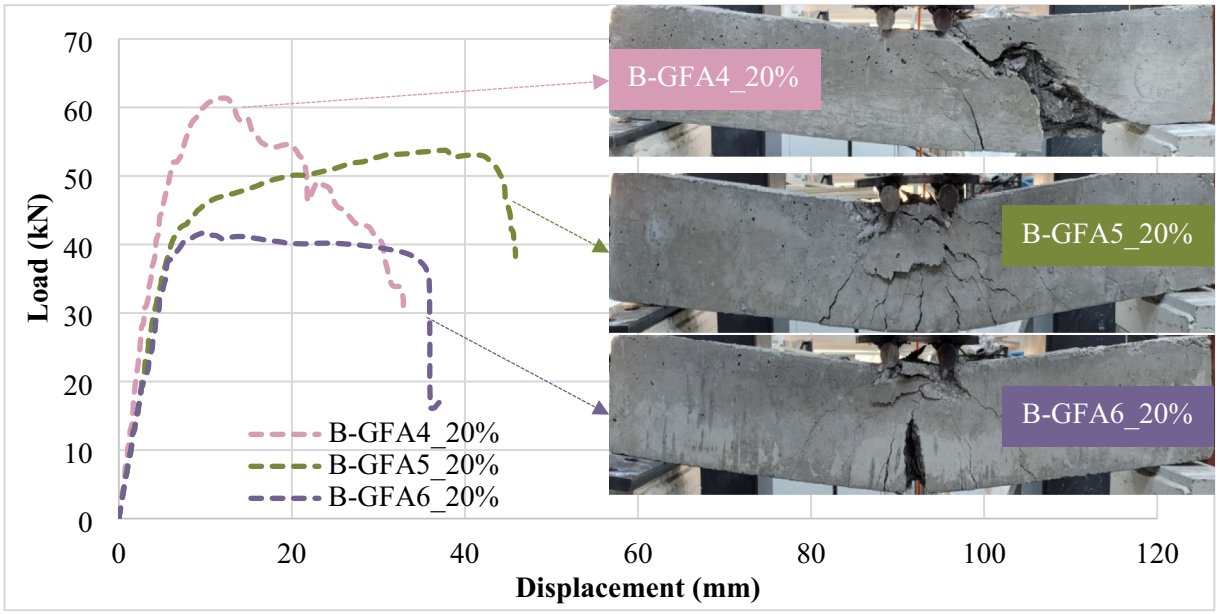

Fig. 9. Load-displacement and failure statement of test examples for B-GFA4_20%, B-GFA5_20%, B-GFA6_20%.

replacement and 10%, 20% FA replacement were designated and tested. Detailed data is presented following subdivisions.

Situation 1: load-bending and fracture performance of different WGA amounts for 2Ø12 longitudinal reinforcement (B-GR1_0%, B-GCA1_10%, B-GCA4_20%)

The impact of different amounts of WGA on fracture and failure behavior of the RCB specimens were specifically inspected. According to this goal, different amounts of WGA were designated as 0%, 10%, and 20% as reinforced longitudinally in the RCB was designated commonly as 2Ø12. According to Fig. 10, when the WGA percentage is selected as 0%, max. load carrying capacity and ultimate displacement were 50.85 kN and 23.45 mm, respectively. On the other hand, the WGA percentage was designated as 10%, the above-mentioned values became 52.63 kN and 13.55 mm, respectively. On the other hand, when the WGA percentage was enhanced to 20%, these values

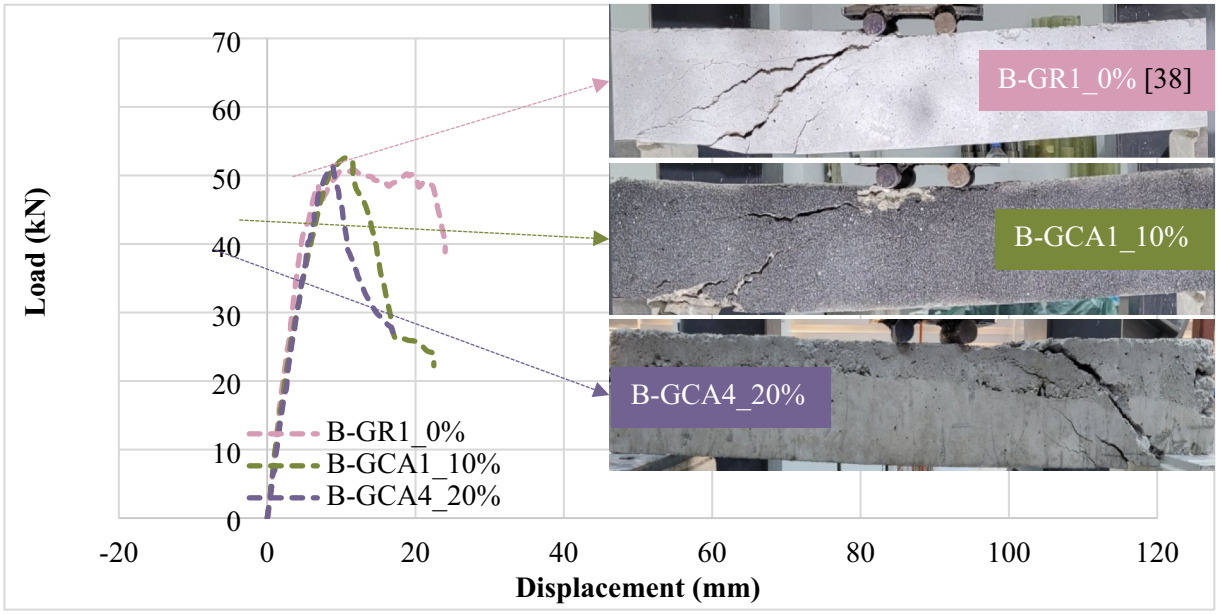

Fig. 10. Load-deformation and failure statement of test examples for B-GR1_0%, B-GCA1_10%, B-GCA4_20%.

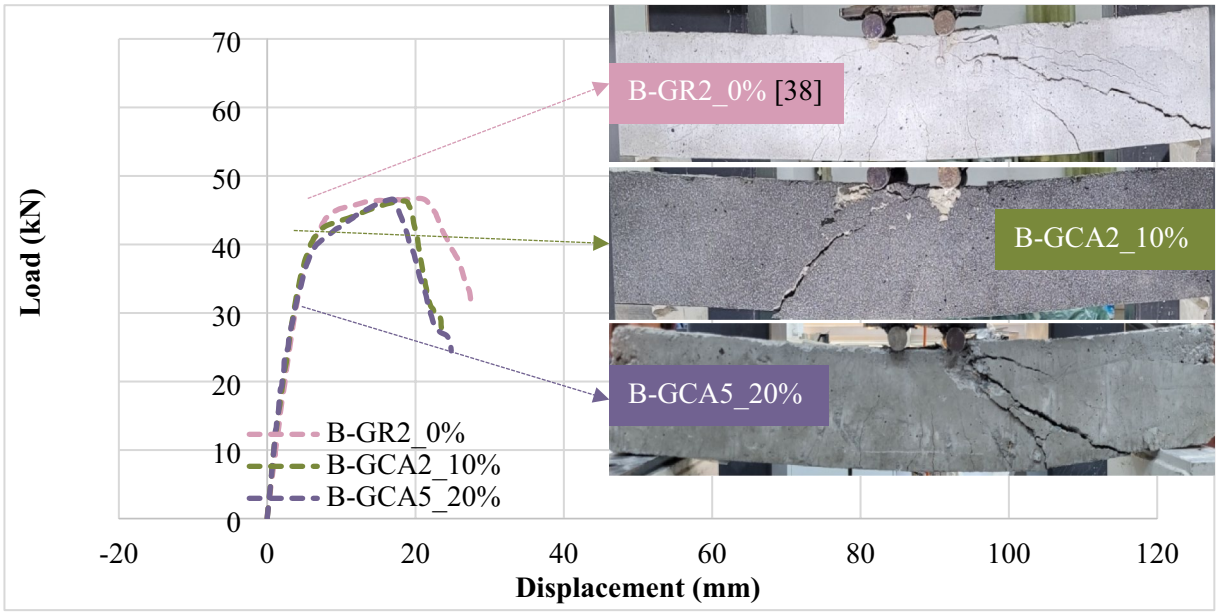

Fig. 11. Load-deformation and failure statement of test examples for B-GR2_0%, B-GCA2_10%, B-GCA5_20%.

decreased to 51.40 kN and 10.28 mm. As observed as a significance of investigational test results for 0%, 10%, 20%, significant bending cracks were detected in the sample based on the vertical load as depicted in Fig. 10.

Situation 2: load-bending and fracture performance of different WGA amounts for 2Ø10 longitudinal reinforcement (B-GR2_0%, B-GCA2_10%, B-GCA5_20%)

In this section, 2Ø10 reinforced longitudinally in the RCB was utilized and WGA percentages were designated as 0%, 10%, and 20% to inspect the influence of altered WGA quantities in the RCB. According to Fig. 11, for the WGA proportion chosen as 0%, max. load carrying capacity and ultimate displacement were 46.72 kN and 24.83 mm. If the WGA proportion was chosen as the 10%, above mentioned values became 46.34 kN and 20.46 mm, respectively. If the WGA proportion improved to 20%, above mentioned values reduced to 46.60 kN and 19.43

mm. As observed from examination tests for 0%, 10%, 20%, the presence of significant bending fractures in the RCB was determined by analyzing the vertical load, as shown in Fig. 11.

Situation 3: load-bending and fracture performance of different WGA amounts for 2Ø8 longitudinal reinforcement (B-GR3_0%, B-GCA3_10%, B-GCA6_20%)

In this part, amounts of WGA were designated as 0%, 10%, and 20%. The 2Ø8 longitudinal reinforcement was employed in the specimen. According to Fig. 12, for the WGA proportions chosen as 0%, max. load carrying capacity and ultimate displacement were 39.32 kN and 52.75 mm. When the WGA proportion was selected as 10%, the above-mentioned values were established as 37.82 kN and 49.68 mm. As the WGA proportion increased to 20%, above mentioned values became 37.89 kN and 48.14 mm, respectively. As detected from the experimental part for 0%, 10%, 20%, Significant bending cracks were observed in the test sample subjected to the vertical load as depicted in Fig. 12. As stated above, as related to these conditions for 2Ø8 strengthened longitudinally in the RCB, the results show that as the ratio of the WGA enhanced from 0% to 20%, the load carrying capacities of the test samples gradually reduced from 39.32 kN to 37.89 kN due to the subsequent development of share cracks in the samples. This is because of the alkali-silica reaction. The chemical process known as the alkali-silica reaction (ASR) occurs when hydroxyl ions in the concrete pore water react with the silica in aggregate[42]. This reaction causes swelling; the resulting pressures induce microcracks in glass particles, which damage the concrete[43,44]. It may also accelerate freeze-thaw damage or corrosion of concrete and structures[45].

However, ASR formation can be prevented through additional measures. The foremost among these is the use of supplementary cementitious materials such as ground granulated blast-furnace slag, natural pozzolans (raw or calcined), fly ash, silica fume, metakaolin, etc., in the concrete mixture[46]. These materials can mitigate harmful expansions caused by ASR. Nevertheless, the appropriate replacement ratio depends on the reactivity of the aggregate and the alkali content of the cement, and should be verified by mixture expansion tests as well as fresh/hardened concrete properties. In addition, annealing the glass before use, employing glass aggregates finer than 0.3 mm, and incorporating lithium-based admixtures can also be effective in reducing and controlling ASR[47].

Situation 4: load-bending and fracture performance of different WGA amounts for 2Ø12 longitudinal reinforcement (B-GR1_0%, B-GFA1_10%, B-GFA4_20%)

To explore the impact of different WGA replacing FA proportions in the RCB, amounts of WGA were chosen as 0%, 10%, and 20%. 2Ø12 longitudinal reinforcement was used in the RCB. According to Fig. 13, for the WGA replacing FA proportions selected as 0%, max. load carrying capacity, and the ultimate displacement were 50.85 kN and 23.45 mm. If the WGA replacing FA proportions was carefully chosen as 10%, this value was measured as 57.10 kN and 16.39 mm. Then, as the WGA replacing FA proportions improved to 20%, the above-mentioned values increased up to 61.37 kN and 21.34 mm. As noticed from test results for 0%, 10%, 20%, significant bending cracks were observed, especially in the sample including the WGA replacing FA proportions selected as 0% as shown in Fig. 13. While compared to coarse aggregate, it is realized that the load-bearing ability of the RCB rises with the addition of FA to the mixture.

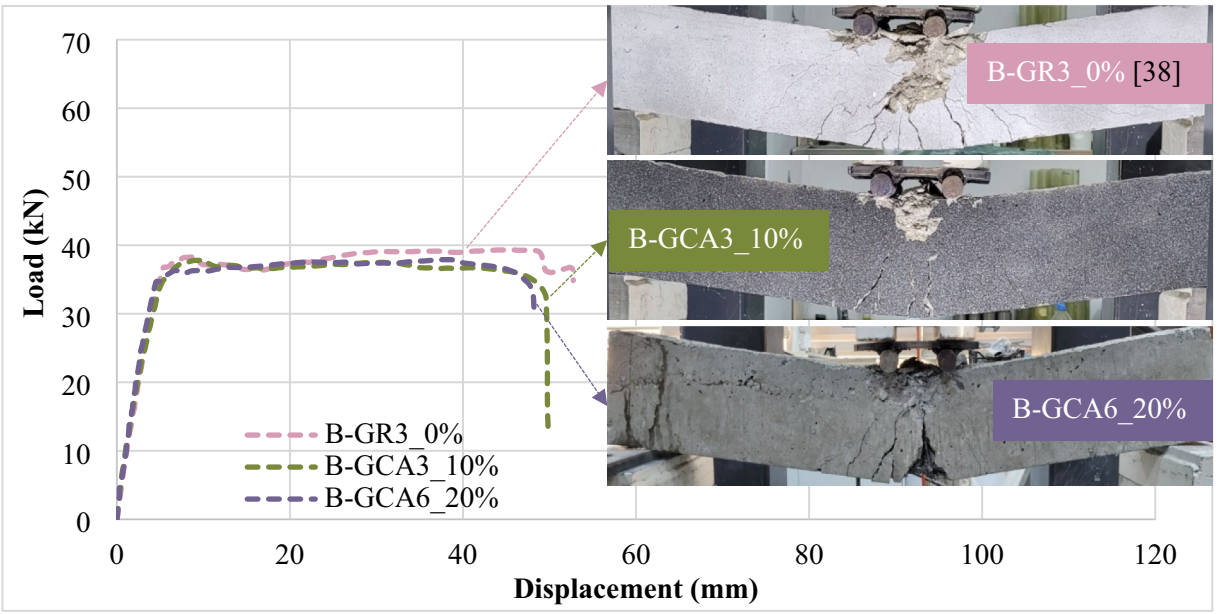

Fig. 12. Load-deformation and failure statement of test examples for B-GR3_0%, B-GCA3_10%, B-GCA6_20%.

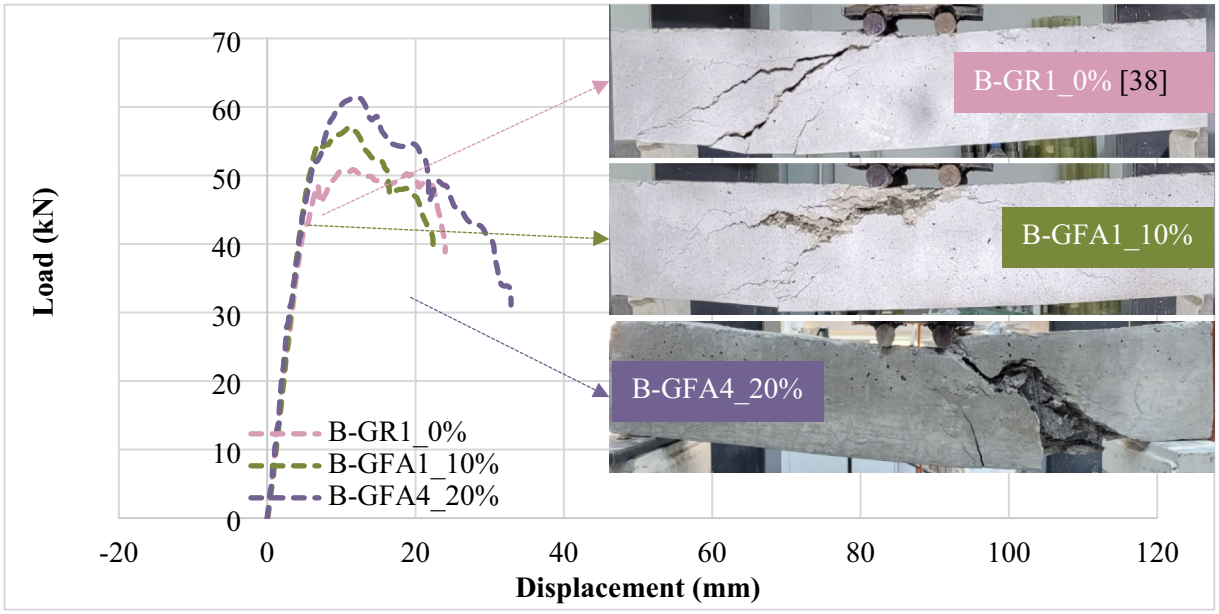

Fig. 13. Load-deformation and failure statement of test examples for B-GR1_0%, B-GFA1_10%, B-GFA4_20%.

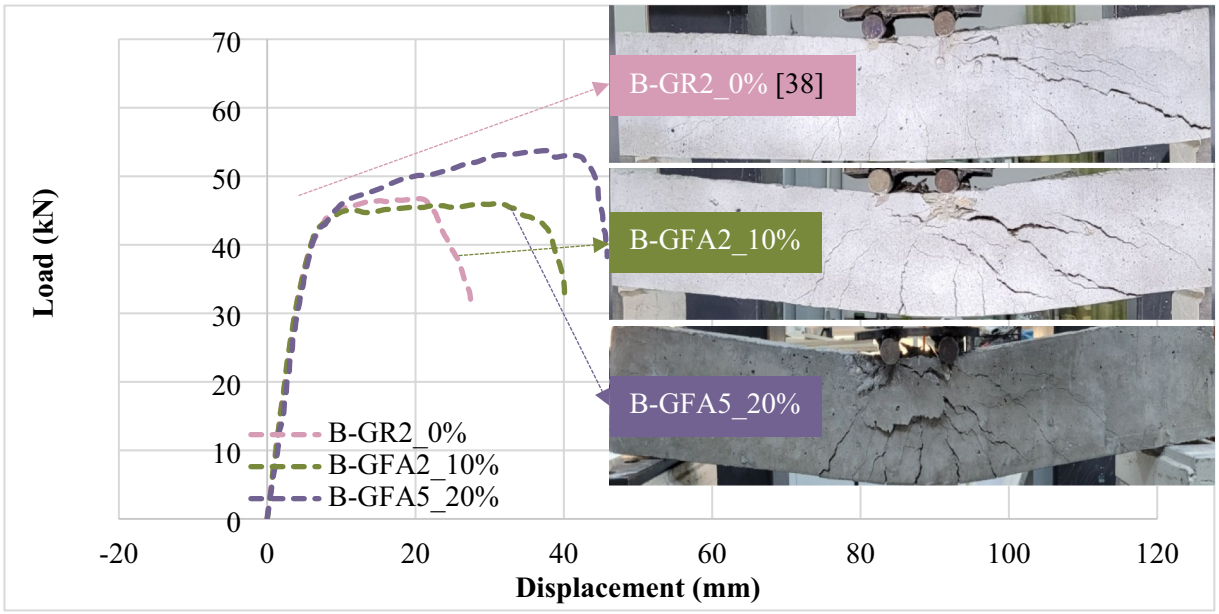

Fig. 14. Load-deformation and failure statement of test examples for B-GR2_0%, B-GFA2_10%, B-GFA5_20%.

Situation 5: load-bending and fracture performance of different WGA amounts for 2Ø10 longitudinal reinforcement (B-GR2_0%, B-GFA2_10%, B-GFA5_20%)

To examine the impact of different WGA replacing FA proportions in the RCB, amounts of WGA were chosen as 0%, 10%, and 20%. On the other hand, the 2Ø10 reinforced longitudinally in the RCB was utilized. According to Fig. 14, for the WGA replacing FA proportions selected as 0%, max. load carrying capacity and ultimate displacement were 46.72 kN and 24.83 mm, respectively. On the other hand, as the WGA replacing FA proportions was carefully chosen as 10% and 20%, above mentioned values were 46.03 kN and 38.81 mm for 10% and 53.75 kN and 44.94 mm for 20%. As observed from the experimental part for 0%, 10%, and 20%, significant bending cracks occurred in the samples, especially in the RCB including the WGA replacing FA proportions selected as 0% as offered in Fig. 14. As mentioned earlier, compared with coarse aggregate, the load-bearing capacity of the RCB rises from 46.72 kN to 53.75 kN with the addition of FA to the mixture.

Situation 6: fracture and load-bending behavior of proportion of WGA for 2Ø10 longitudinal reinforcement (B-GR3_0%, B-GFA3_10%, B-GFA6_20%)

To observe the effect of different WGA replacing FA proportions in the RCB, amounts of WGA were chosen as 0%, 10%, and 20%. Additionally, the 2Ø8 reinforced longitudinally in the RCB was employed. According to Fig. 15, for the WGA replacing FA proportions designated as 0%, max. load carrying capacity and ultimate displacement were 39.32 kN and 52.75 mm. On the other hand, as the WGA replacing FA proportions were carefully selected as 10% and 20%, above mentioned values were observed as 40.89 kN and 41.19 mm for 10% and 41.72 kN and 35.81 mm for 20%. As detected from the experimental part for 0%, 10%, and 20%, significant bending cracks occurred, especially in the test sample including the WGA replacing FA proportions selected as 0% as presented in Fig. 15.

Other studies on reinforced concrete beams have also shown that waste glass aggregate (WGA) can enhance shear and flexural strength; for example, beams containing 10–15% WGP exhibited strength improvements, whereas a decrease was observed at 20% WGP[18]. From the perspective of design codes, Eurocode 2 and ACI 318 are based on natural aggregate concrete mixtures; the integration of WGA into these codes is currently limited. However, the literature demonstrates how WGA affects the elastic modulus and strength of concrete, highlighting the importance of adapting these effects into design parameters[37]. In conclusion, the use of WGA in reinforced concrete beams is feasible, providing environmental benefits while maintaining strength. Nevertheless, further field and experimental studies are required to determine the optimal replacement ratios and ensure compliance with design codes.

Calculation of bending capacities of the test specimens and comparison with experimental results

In the study, to calculate the bending capacities of the beams, the maximum cross-sectional bearing strength of the beams was calculated with the help of the numerical analysis method. Microsoft Excel and Visual Basic for Applications (VBA) programs were utilized in the calculation of beam section bearing forces and numerical analysis. For the numerical analyses, an algorithm was developed in such a way that deformations in the fiber were incrementally increased until the extreme (top) concrete fiber was crushed, and the compatibility (Eqs. 1–2) and equilibrium (Eqs. 3–7) equations are re-established for each step.

$$c_i = \frac{\varepsilon_{ci} d}{\varepsilon_{ci} + \varepsilon_{si}} \tag{1}$$

$$c_i = \frac{\varepsilon_{ci} d'}{\varepsilon_{ci} - \varepsilon_{si}'} \tag{2}$$

$$F_{si} = F'_{si} + F_{ci} \tag{3}$$

$$F_{si} = A_s f_{si} \tag{4}$$

$$F'_{si} = A'_s f'_{si} \tag{5}$$

$$F_{ci} = f_{cmi} b_w c_i k_i \tag{6}$$

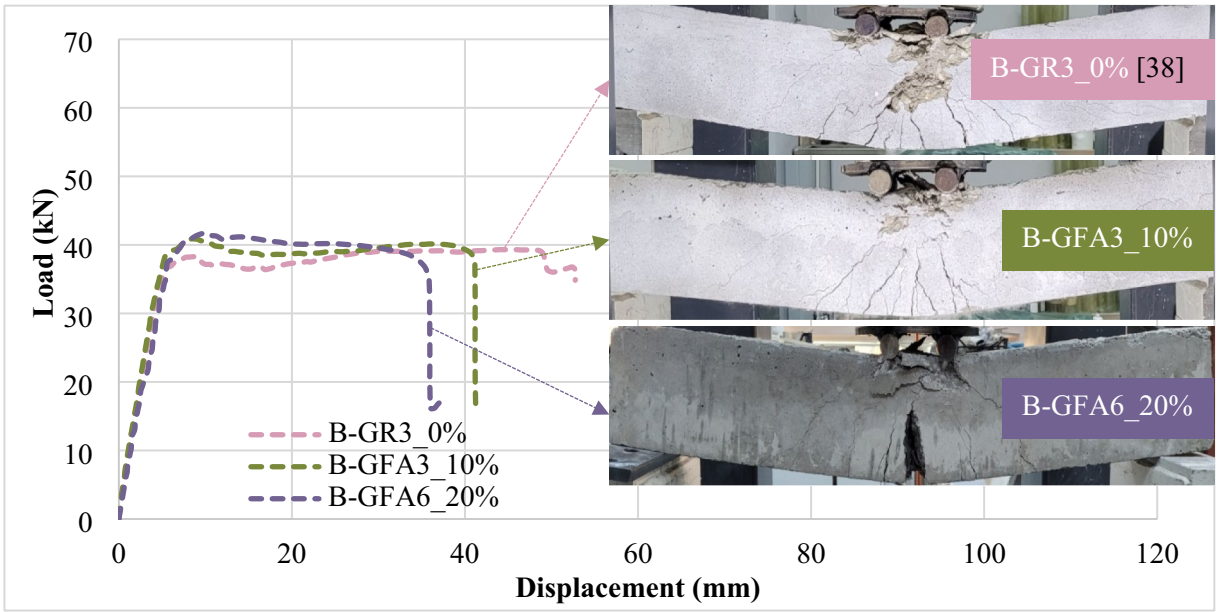

Fig. 15. Load-deformation and failure statement of test examples for B-GR3_0%, B-GFA3_10%, B-GFA6_20%.

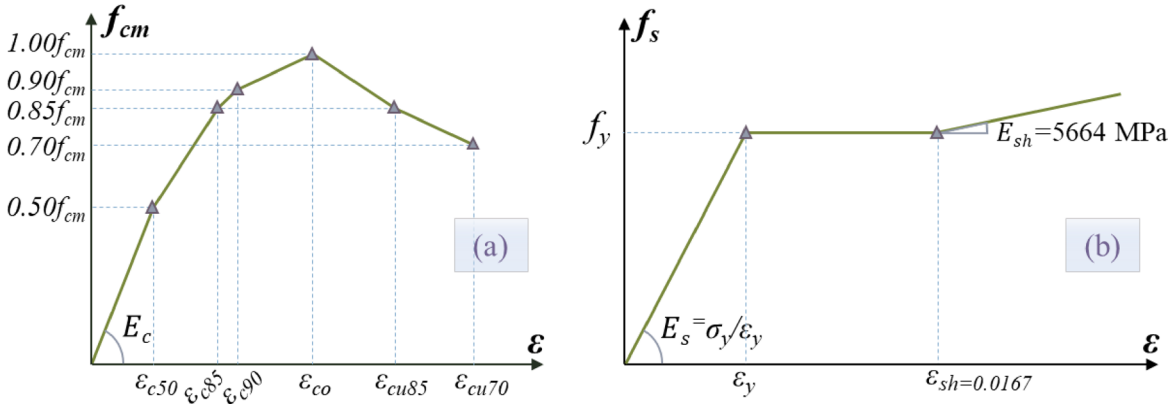

Fig. 16. (**a**) Concrete model suggested by Ispir et al.(adapted from[48]; (**b**) Idealized trilinear steel model).

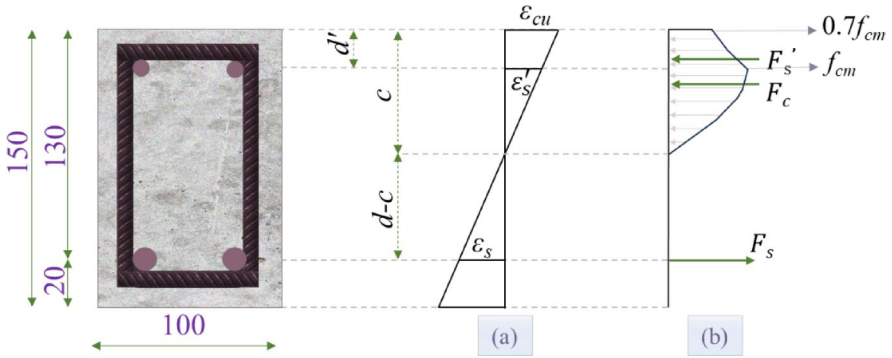

Fig. 17. (**a**) Strain diagram of the beam section under ultimate load; (**b**) Stress diagram of the beam section under ultimate load.

$$M_{NAi} = F_{si}\,(d - c_i) + F'_{si}\left(c_i - d'\right) + F_{ci}m \tag{7}$$

$$P_{NAi} = \frac{2M_{NA}}{a} \tag{8}$$

where, c_i is the neutral axis depth at step i (mm), ε_{ci} is the concrete compressive strain at step i, d is the effective depth (mm), ε_{si} is the tensile reinforcement strain at step i, ε_{si}' is the compressive reinforcement strain at step i, F_{si} is the tensile reinforcement force at step i (N), F_{si}' is the compressive reinforcement force at step i (N), F_{ci} is the concrete compressive force at step i (N), A_s is the tensile reinforcement area (mm^2), A_s' is the compressive reinforcement area (mm^2), f_{si} is the tensile reinforcement stress at step i (MPa), f_{si}' is the compressive reinforcement stress at step i (MPa), f_{cmi} is the concrete cylinder compressive strength at step i (MPa), k_i is the coefficient of equivalent rectangular concrete area at step i, m is the distance from the neutral axis to the center of the concrete compressive force at step i (mm), M_{NAi} is the moment value of the beam section at step i (Nmm), P_{NAi} is the load bearing value of the beam at step i (N), a is the beam shear span (mm).

To accurately reflect the stress and strain relationship of concrete in the analyses, the stress-strain curve recommended by Ispir et al.[48] for concretes with low compressive strength was used. The curve suggested by Ispir et al.[48] was shown in Fig. 16 and the coordinates of the curve were presented in Eqs. 9–15.

In the analysis, an idealized trilinear stress-strain model was used for the stress-strain relationship of steel reinforcement. This model is presented in Fig. 16. In the model, ε_y = yield strain of steel (%), f_y = yield stress of steel (MPa), E_s = modulus of elasticity (MPa), ε_{sh} = initial-strain hardening (%), E_{sh} = hardening modulus of elasticity. The yield strengths of the reinforcement are 560, 550, 510, and 450 MPa for reinforcement with diameters of 6, 8, 10 and 12 mm, respectively. In addition, in the analyses, it was assumed that the elastic moduli of all reinforcement were 200,000 MPa. For hardening modulus of elasticity (E_{sh}) and strain values (ε_{sh}), statistical average values of 5664 MPa and 0.0167 for steel reinforcement recommended by Carrillo et al.[49] were used. The stress-strain diagrams obtained in the beam section under ultimate load are presented in Fig. 17a and b.

$$\epsilon_{c50} = 0.00008 f_{cm}^{0.55} \tag{9}$$

$$\epsilon_{c85} = 0.0002 f_{cm}^{0.58} \tag{10}$$

$$\epsilon_{c90} = 0.0003 f_{cm}^{0.52} \tag{11}$$

$$\epsilon_{co} = 0.001 f_{cm}^{0.25} \tag{12}$$

$$\epsilon_{cu85} = 0.0074 f_{cm}^{-0.23} \tag{13}$$

$$\epsilon_{cu70} = 0.0122 f_{cm}^{-0.29} \tag{14}$$

$$E_c = 5345 f_{cm}^{0.5} \tag{15}$$

where, f_{cm} is the average cylinder concrete compressive strength (MPa); ε_{c50}, ε_{c85}, ε_{c90}, ε_{co}, ε_{cu85} and ε_{cu70} are the strain values of concrete under compressive stress values of $0.5f_{cm}$, $0.85f_{cm}$, $0.90f_{cm}$, $1.00f_{cm}$, $0.85f_{cm}$, $0.70f_{cm}$ respectively. E_c is the modulus of elasticity of concrete (MPa). Equations (17–20) given in ACI 318 – 19[50] have been used to calculate the shear capacities of normal-weight concrete beams. ACI 318 – 19[50] proposes a shear strength equation (V) where the influence of concrete (V_c) and stirrups (V_s) to the shear strength are taken into account. When calculating the concrete contribution (V_c) in the model, it is assumed that longitudinal reinforcement also contributes to the shear strength of concrete.

$$V_c = 0.66 \sqrt[3]{\rho_w} \sqrt{f_c} b_w d \qquad A_v \geq 0.35 \frac{b_w}{f_{yt}} s \tag{16}$$

$$V_s = \frac{A_v f_{yt}}{s} d \tag{17}$$

$$V = V_c + V_s \leq V_c + V_{s,max} \tag{18}$$

$$V_{c,max} = 0.42 \sqrt{f_c} b_w d \tag{19}$$

$$V_{s,max} = 0.66 \sqrt{f_c} b_w d \tag{20}$$

Where, V_c is the shear strength obtained from concrete (N), V_s is the shear strength obtained from transverse reinforcement (N), V is the total shear strength (N), f_c is compressive strength (MPa) of the cylindrical concrete test samples, $\rho_w = A_s/b_w d$, A_s is the area of the tensile reinforcement (mm^2), b_w is the beam width (mm), d is the effective depth of the beam (mm), f_{yt} is the transverse reinforcement yield strength (MPa), s is the distance between the transverse reinforcements (mm).

A comparison of the calculated shear and bending capacities of the beams with the test results was given in Table 2. As shown in Table 2, the calculated share capacities of all beams are at least 44% (B-GFA4_20%) greater than the experimental shear capacities. Moreover, the calculated shear capacities of all beams are at least 44% larger than the shear force corresponding to the calculated bending capacities. This confirms that sufficient stirrups have been placed in the beams against shear failure.

However, shear failure occurred in some of the beams due to the spread of the shear crack before the bending capacity was reached. In some beams, pseudo-bending failure occurred as a result of the spread of the shear

Test ID	V_c (kN)	$V_{c,max}$ (kN)	V_s (kN)	$V_{s,max}$ (kN)	V_{ACI} (kN)	$V_{exp.}$ (kN)	V_{Exp}/V_{ACI}	P_{Exp} (kN)	P_{NA} (kN)	P_{Exp}/P_{NA}	Failure Type*
B-GR1_0% [38]	8.64	21.22	41.17	33.35	41.99	25.43	0.61	50.85	60.29	0.84	PS
B-GR2_0% [38]	7.65	21.22	41.17	33.35	41.00	23.36	0.57	46.72	49.87	0.94	PS
B-GR3_0% [38]	6.59	21.22	41.17	33.35	39.94	19.66	0.49	39.32	36.15	1.09	F
B-GCA1_10%	8.59	21.09	41.17	33.14	41.73	26.31	0.63	52.63	60.19	0.87	S
B-GCA2_10%	7.61	21.09	41.17	33.14	40.75	23.17	0.57	46.34	49.80	0.93	PS
B-GCA3_10%	6.55	21.09	41.17	33.14	39.70	18.91	0.48	37.82	36.11	1.05	F
B-GCA4_20%	8.37	20.56	41.17	32.31	40.68	25.70	0.63	51.40	59.74	0.86	S
B-GCA5_20%	7.41	20.56	41.17	32.31	39.72	23.30	0.59	46.60	49.51	0.94	PS
B-GCA6_20%	6.39	20.56	41.17	32.31	38.70	18.95	0.49	37.89	35.96	1.05	F
B-GFA1_10%	8.69	21.35	41.17	33.55	42.24	28.55	0.68	57.10	60.40	0.95	PS
B-GFA2_10%	7.70	21.35	41.17	33.55	41.25	23.01	0.56	46.03	49.95	0.92	F
B-GFA3_10%	6.63	21.35	41.17	33.55	40.18	20.45	0.51	40.89	36.18	1.13	F
B-GFA4_20%	9.10	22.36	41.17	35.13	44.24	30.68	0.69	61.37	61.33	1.00	PS
B-GFA5_20%	8.06	22.36	41.17	35.13	43.20	26.87	0.62	53.75	50.50	1.06	F
B-GFA6_20%	6.95	22.36	41.17	35.13	42.08	20.86	0.50	41.72	36.43	1.15	F

Table 2. Calculated shear and bending capacities of beams. *S is the Shear failure, PS is the Pseudo Bending failure, F is the bending failure. The theoretical calculations of the reference beams are calculated with the equations presented in this paper.

crack before reaching sufficient ductility after the beams reached their moment capacity. This situation occurred due to one or a combination of three possible reasons. Firstly, it is due to the very high shear demand of the beam due to the low ratio of shear span to effective beam height (a/d = 2.69). As it is known, as the a/d ratio approaches approximately 2.5, the shear strength required from the beam increases to its maximum level[51]. The second is because as the reinforcement ratio in the beams increases, more shear strength is required from the beams due to the increasing bending capacity of the beams. The stirrup ratios of all beams tested in the study are the same. The third is the change in the compressive, splitting, and bending strengths of concrete depending on the replacement rate of glass aggregate with normal aggregate. As the amount of replacement of coarse glass aggregate with coarse normal aggregate increased, the concrete compressive, splitting, and bending strengths gradually decreased, and as the shear strength of the concrete decreased, the shear strength of the beams also decreased. However, as the replacement ratio of fine glass aggregate with fine normal aggregate increased, the compressive, splitting, and bending strengths of concrete gradually increased and the shear strength of concrete increased greater than anticipated. Experimental bending properties are given in Table 3.

As can be seen from Tables 2 and 3; Figs. 6 and 7, shear failure occurs in beams with coarse glass aggregates because the beams with a high reinforcement ratio (1.74%) cannot meet the increasing shear demand. For this reason, the expected theoretical strengths in these beams were not achieved and the experimental strengths were 13% to 14% lower than the theoretical strengths. In beams with a medium reinforcement ratio (1.21%), pseudo-bending failure occurred in the beams since the shear strength required from the beams was lower. In these beams, the experimental strengths differ from the theoretical strengths by only 6% to 7%, showing close agreement between experimental and theoretical results. In beams with a low reinforcement ratio (0.77%), bending failure occurred in the beams since the shear strength required from the beams was the lowest. It is seen that the experimental strengths in these beams are 5% greater than the theoretical strengths and are very close to them.

In Tables 2 and 3, the theoretical and experimental strengths of fine glass aggregate beams are compared. Although the beams with a high reinforcement ratio (1.74%) met the increasing shear demand to a small extent, pseudo-bending failure occurred in the beams due to shear cracks after the yield strength of the beams was reached (Figs. 8 and 9). Since the experimental strengths of these beams differ from the theoretical strengths by up to 5%, the results are quite close. In beams with medium and low reinforcement ratios (1.21% and 0.77%), bending failure occurred in the beams because the shear strength required from the beams was low (Figs. 8 and 9). Experimental strengths in these beams were between 6% and 15% higher than theoretical strengths (except B-GFA2_10% beam).

Assessment of the experimental crack and displacement reflection using digital image correlation

The microcracks and fleuxural behavior of concrete[52] have all been examined using the digital image correlation approach in recent works. As shown in detail in Fig. 4, the picture was captured during the experimental testing using an imaging device (Nikon D5300), a LED lamp (80w), and a laptop computer. A digital camera with a resolution of 24.2 megapixels was used to take photographs of the RCB throughout the experimental testing phase. This was done in addition to the loading phase, during which no notable fractures were observed elsewhere. Image capture was carried out from this location during the whole of the experiment. The digital camera was mounted on a tripod such that its axis was perpendicular to the attention region. Furthermore, the digital camera is configured to capture an image every four seconds using the image capture speed setting. For

Test specimens	P_{max} (kN)	δ_y (mm)	δ_{Pmax} (mm)	δ_u (mm)	Ductility ratio (δ_u/δ_y)	Failure type	Ductility level
B-GR1_0% [38]	50.85	5.57	11.56	23.45	4.21	Pseudo Bending	Partially Sufficient
B-GR2_0% [38]	46.72	5.83	20.44	24.83	4.26	Pseudo Bending	Partially Sufficient
B-GR3_0% [38]	39.32	4.54	44.73	52.75	11.61	Bending	Sufficient
B-GCA1_10%	52.63	6.88	10.69	13.55	1.97	Shear	Deficient
B-GCA2_10%	46.34	5.69	18.37	20.46	3.60	Pseudo Bending	Deficient
B-GCA3_10%	37.82	4.58	10.12	49.68	10.84	Bending	Sufficient
B-GCA4_20%	51.40	5.32	8.92	10.28	1.93	Shear	Deficient
B-GCA5_20%	46.60	6.41	16.89	19.43	3.03	Pseudo Bending	Deficient
B-GCA6_20%	37.89	4.07	37.73	48.14	11.84	Bending	Sufficient
B-GFA1_10%	57.10	5.42	11.20	16.39	3.02	Pseudo Bending	Deficient
B-GFA2_10%	46.03	5.66	31.37	38.81	6.86	Bending	Sufficient
B-GFA3_10%	40.89	4.63	8.48	41.19	8.90	Bending	Sufficient
B-GFA4_20%	61.37	6.82	12.10	21.34	3.13	Shear	Deficient
B-GFA5_20%	53.75	9.82	37.41	44.94	4.58	Bending	Sufficient
B-GFA6_20%	41.72	5.44	9.95	35.81	6.59	Bending	Sufficient

Table 3. Experimental bending properties and collapse behavior of beams. P_{max} is the maximum load; δ_y is the yield displacement at the $0.85P_{max}$; δ_{Pmax} is the maximum displacement at the P_{max}; δ_u is the ultimate displacement at the $0.85P_{max}$.

the purpose of enhancing the photographs, external lightening was used using the beam placed on the front surface of the element. Black and white paint was applied on the RCBs so that cracks could be easily identified throughout the imaging process. This was done in order to process the images. It is possible to convert the grid displacements obtained from digital photographs into the real displacement of the RCB specimen, which may be shown in Fig. 18.

The color variation demonstrates its displacement in the Y direction in Fig. 18. As a result of observing this graph, it is possible to see that the bottom of the RCB exhibited the most negative displacement values. Figure 18 illustrates how this assertion lends credence to the divergence of the actual RCB sample, which was situated beneath the loading point. A representation of the reference locations that were occupied on the RCB during imaging is shown in Fig. 18-a. Although the loading is close to the collapse load, the angular displacement figure presents what appears to be a dividing line at its lowest point. Furthermore, as can be seen in Fig. 19, the digital picture of the specimen reveals the presence of a little cracking on the surface of the RCB, which is dependent on the strain values. A further observation that can be made from the figure is that the cracking has caused the RCB test specimen to spall.

Figure 20 illustrates that the RCB example is fractured due to collapse loading, and the separation location is parallel, as the potential division location is evident during the loading phase. Figure 20 also shows that all strains are uniformly distributed while the load was applied, the crack has not been recognized in the RCB specimen yet. As the load is gradually increased, the strain measurement reveals slight strain concentration near the bottom of the RCB in the y direction. When the loading is improved, it has been detected that cracks not visible to the naked eye.

The strain density at the conclusion of the tests for the RCB specimen exposed to collapse loading is nearly the same as those for specimens depending on lower loadings, and it reaches the whole specimen as shown in Fig. 20. The assessment of the displacement values that were observed from measurements and digital image correlation is provided at the conclusion of the digital image correlation procedures, as shown in Fig. 20. The results of the experimental investigations and digital image correlation are more closely related, as illustrated in Fig. 21.

Conclusion

This investigational analysis studied the effects of different WGA percentages on the flexural behavior of RCB test samples including altered strengthened longitudinally. A series of tests consisting of a total of 12 samples were performed and these tests were compared with 3 reference beams made before[38]. The obtained results are briefly summarized as follows:

- When the proportion of WGA substituting FA was increased up to 20%, a significant increase in compressive strength was observed compared to the reference sample (0% WGA). This increase can be attributed to the binding property of WGA.
- When the proportion of WGA substituting CA reached 20%, there was a significant decrease in compressive strength compared to the reference concrete. The decrease in compressive strength can be explained by two reasons: The first, WGA has a smoother surface compared to normal aggregates, which leads to a weakening

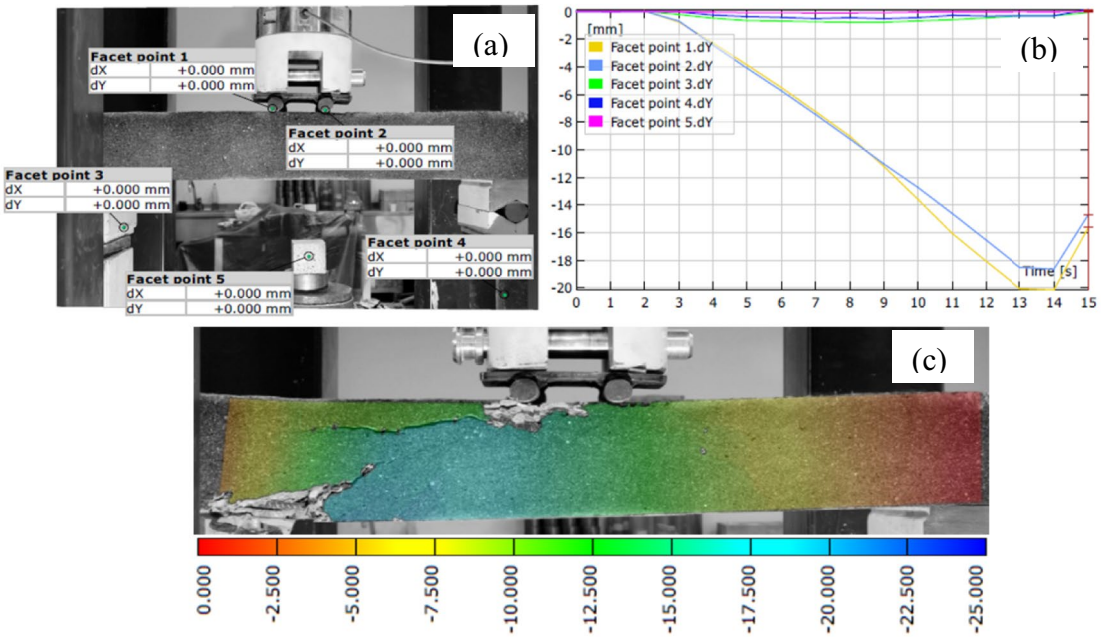

Fig. 18. (**a**) Digital imaging involves the use of reference points.; **(b)** under-load imaging techniques; **(c)** digital imaging-derived deformation graph.

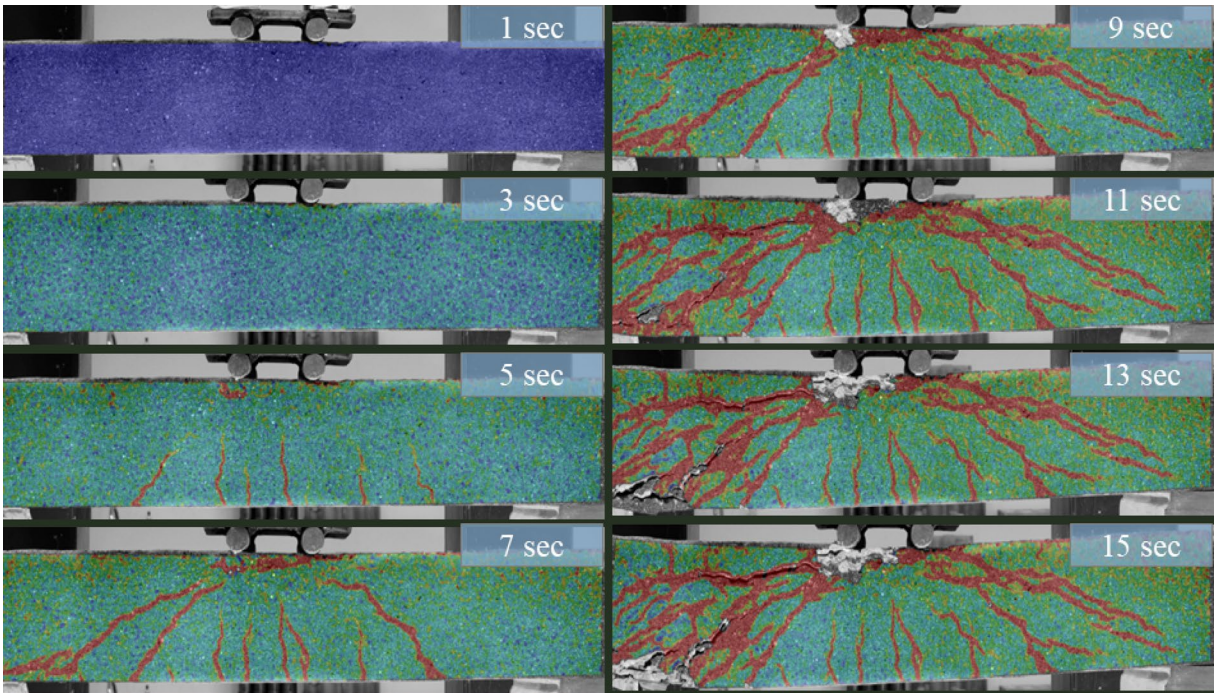

Fig. 19. Comparison of the digital image correlation crack observation for times.

of the bond between the aggregates and the cement matrix. This effect is more pronounced as the glass content increases. The second, the water absorption capacity of WGA is lower than that of normal aggregates. This results in higher slump values in the mix; when the extra free water evaporates, voids form in the concrete and the compressive strength decreases.

- The structural behavior of the experimentally investigated RCBs improved with the use of WGA; first crack formation and maximum load capacity were consistently increased. However, a reduction in deformation was observed at the first fracture and maximum load levels.
- According to the experimental test results, the maximum bearing capacity of RCB specimens increased with increasing WGA content in the concrete mix. When RCB test specimens with different WGA amounts were compared, the maximum deflection occurred in the middle of the test specimens, in B-GFA5_20% RCBs containing 20% WGA.
- When the test samples were examined, it was observed that the addition of FA to the mix increased the load-carrying capacity compared to coarse aggregate.
- In the study, the maximum sectional bearing capacity of concrete beams containing WGA was also determined by numerical analysis and a maximum difference of 15% was observed between the calculated values and the experimental results. However, this difference changed from a positive value (+15%) to a negative value (−13%) as the failure mode of the beams changed from flexural failure to shear failure with the increase in the proportion of tensile reinforcement in the section.
- In addition to utilizing WGA as a resource and improving the mechanical properties of concrete, the use of WGA in concrete can contribute to the protection of the ecological environment and provide an important support to the sustainable development of the construction industry.

This study shows that the use of WGA improves the mechanical performance of reinforced concrete beams and contributes to sustainable construction practices. In future studies, the effects of different WGA ratios on long-term strength and durability can be investigated in detail. Furthermore, the performance of WGA under different concrete mix designs, environmental conditions and loading types can be investigated. The practical application of WGA lightweight aggregates and bricks as building materials is important to verify their economic and ecological benefits. In addition, further experimental and numerical studies on the ASR potential of WGA, optimum replacement rates and its integration into design codes are recommended.

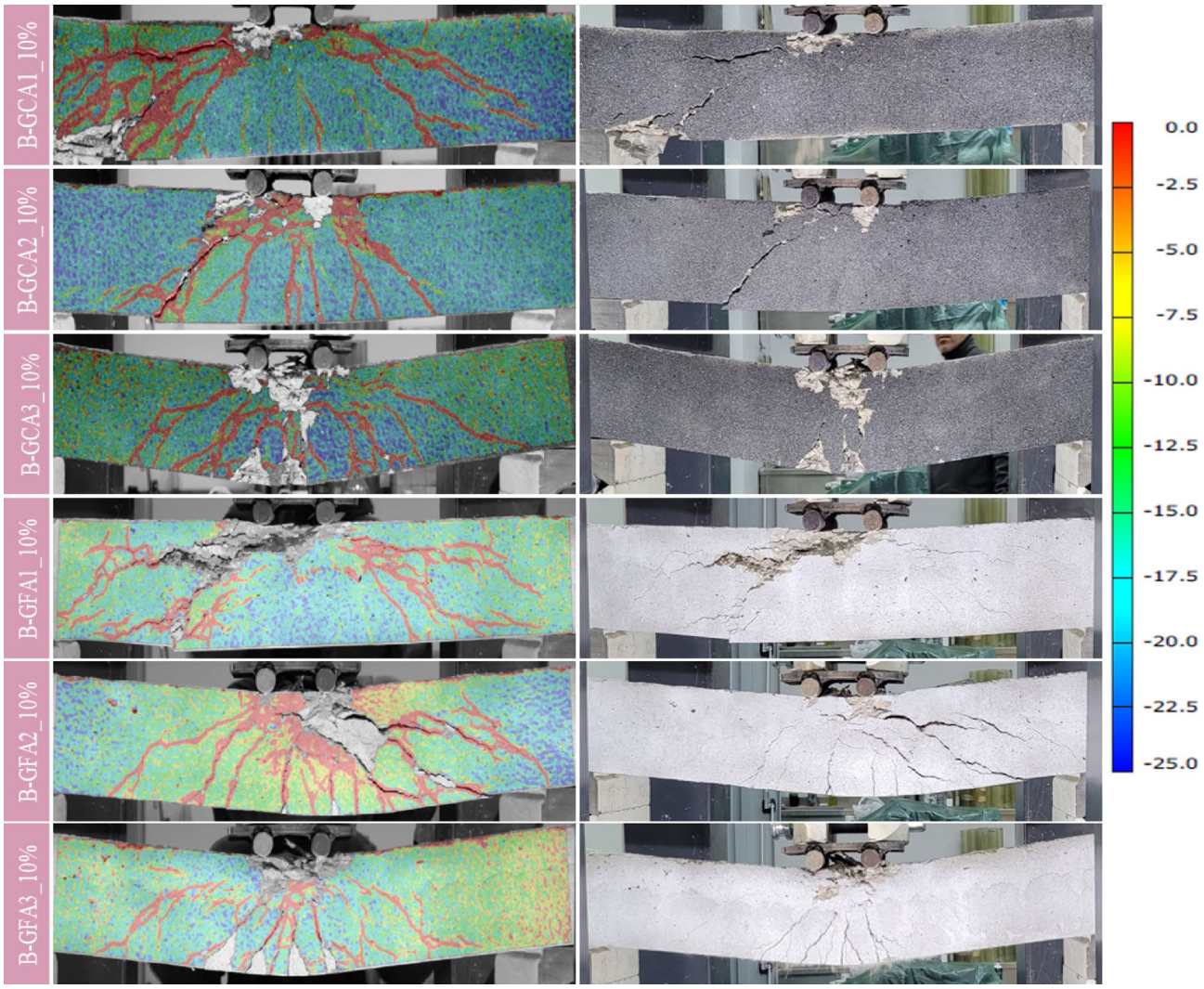

Fig. 20. Assessment of the experimental crack reflection and digital image correlation.

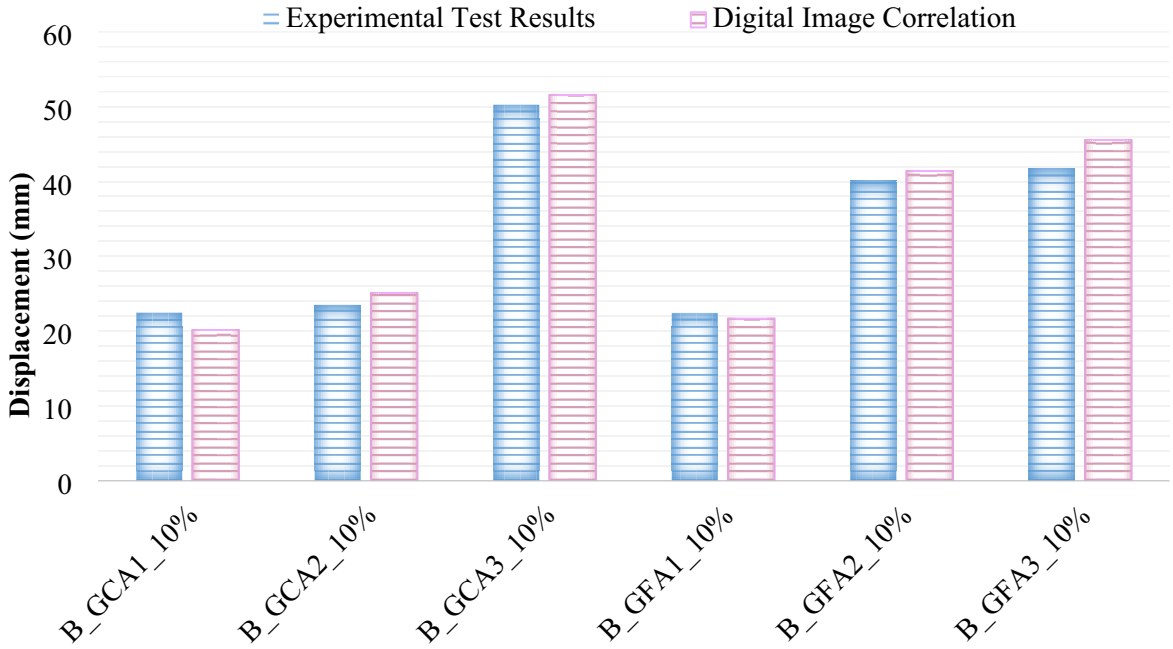

Fig. 21. Assessment of the displacement values at the end of the experiments and digital image correlation.

Data availability

The datasets generated and/or analyzed during the current study are available from the corresponding authors on reasonable request.

Received: 25 July 2025; Accepted: 16 September 2025
Published online: 21 October 2025

References

1. Zhang, F., Lu, Z. & Wang, D. Working and mechanical properties of waste glass fiber reinforced self-compacting recycled concrete. *Constr. Build. Mater.* **439**, 137172 (2024).
2. Miah, M. J. et al. Performance of eco-friendly concrete made from recycled waste tire fine aggregate as a replacement for river sand. *Structures* **58**, 105463 (2023).
3. Liu, S., Zheng, W. & Wu, F. Preparation of ultra-high performance concrete containing waste foundry sand and its application in structures. *Structures* **58**, 105472 (2023).
4. Qaidi, S. et al. Concrete containing waste glass as an environmentally friendly aggregate: A review on fresh and mechanical characteristics. *Materials* **15**(18), 6222. https://doi.org/10.3390/ma15186222 (2022).
5. Özkılıç, Y. O. et al. The use of crushed recycled glass for alkali activated fly Ash based geopolymer concrete and prediction of its capacity. *J. Mater. Res. Technol.* **24**, 8267–8281 (2023).
6. Surendran, H. & Akhas, P. K. Properties of high-performance concrete incorporating toughened glass waste coarse aggregate: an experimental study. *Structures* **60**, 105897 (2024).
7. Harrison, E., Berenjian, A. & Seifan, M. Recycling of waste glass as aggregate in cement-based materials. *Environ. Sci. Ecotechnology*. **4**, 100064 (2020).
8. Batayneh, M., Marie, I. & Asi, I. Use of selected waste materials in concrete mixes. *Waste Manage.* **27** (12), 1870–1876 (2007).
9. Tejaswi, S. S. et al. Experimental investigation of waste glass powder as partial replacement of cement and sand in concrete. *IUP J. Struct. Eng.* **8** (4), 14 (2015).
10. Khan, M. N. N. & Sarker, P. K. Effect of waste glass fine aggregate on the strength, durability and high temperature resistance of alkali-activated fly Ash and GGBFS blended mortar. *Constr. Build. Mater.* **263**, 120177 (2020).
11. Ahmad, J. et al. Concrete with partial substitution of waste glass and recycled concrete aggregate. *Materials* **15** (2), 430 (2022).
12. Dinh, N. H. et al. Tensile performance and cracking characteristics of sustainable textile-reinforced cementitious composites utilizing expanded glass aggregate and fly Ash replacement. *Constr. Build. Mater.* **425**, 136084 (2024).
13. Al-Bawi, R. K., Kadhim, I. T. & Al-Kerttani, O. Strengths and failure characteristics of self-compacting concrete containing recycled waste glass aggregate. Advances in Materials Science and Engineering, 2017. (2017).
14. Arivalagan, S. & Sethuraman, V. Experimental study on the mechanical properties of concrete by partial replacement of glass powder as fine aggregate: An environmental friendly approach. Materials Today: Proceedings, 45: pp. 6035–6041. (2021).
15. Adaway, M. & Wang, Y. Recycled glass as a partial replacement for fine aggregate in structural concrete–Effects on compressive strength. *Electron. J. Struct. Eng.* **14** (1), 116–122 (2015).
16. Topçu, İ. B. & Canbaz, M. Properties of concrete containing waste glass. *Cem. Concr. Res.* **34** (2), 267–274 (2004).
17. Hachemi, S., Khattab, M. & Benzetta, H. Enhancing the performance of concrete after exposure to high temperature by coarse and fine waste fire brick: an experimental study. *Constr. Build. Mater.* **368**, 130356 (2023).
18. Hama, S. M., Mahmoud, A. S. & Yassen, M. M. Flexural behavior of reinforced concrete beam incorporating waste glass powder. *Structures* **20**, 510–518 (2019).
19. Mustafa, T. S., El, S. A., Beshlawy & Nassem, A. R. Experimental study on the behavior of RC beams containing recycled glass. *Constr. Build. Mater.* **344**, 128250 (2022).
20. Hamid, R. & Zubir, M. A. The Flexural Properties of Reinforced Recycled Glass Concrete Beam. Trans Tech Publ. (2014).

21. Atoyebi, O. D. & Sadiq, O. M. Experimental data on flexural strength of reinforced concrete elements with waste glass particles as partial replacement for fine aggregate. *Data Brief.* **18**, 846–859 (2018).
22. Sadiq, O. & Atoyebi, O. D. Flexural strength determination of reinforced concrete elements with waste glass as partial replacement for fine aggregates. *NSE Tech. Trans.* **49** (2), 74–81 (2015).
23. Omer, B. & Saeed, J. Evaluating the Shear Performance of Reinforced Concrete Beams Using Waste Glass Powder as a Sustainable Cement Substitute. *Struct. Concr.* **25**(6), 4812–4832. https://doi.org/10.1002/suco.202301002 (2024).
24. Haido, J. H., Zainalabdeen, M. A. & Tayeh, B. A. Experimental and numerical studies on flexural behavior of high strength concrete beams containing waste glass. *Adv. Concrete Constr.* **11** (3), 239–253 (2021).
25. Legese, A. M. et al. Experimental study on the suitability of waste plastics and glass as partial replacement of fine aggregate in concrete production. *Constr. Mater.* **4** (3), 581–596 (2024).
26. Omer, B. & Saeed, J. Investigating the flexural strength characteristics of reinforced concrete beams utilising waste glass powder as a sustainable cement alternative. *Innovative Infrastructure Solutions*. **9** (6), 1–18 (2024).
27. Safi, H. U., Behsoodi, M. M. & Sharifi, M. N. A comparative analysis of compressive and flexural strength in concrete with partial cement replacement using waste glass powder. *Indonesian J. Mater. Res.* **2** (1), 16–22 (2024).
28. Ji, Z. et al. Research on the flexural performance of recycled coarse aggregate concrete beams after carbonation. *J. Building Eng.* **97**, 110645 (2024).
29. Hama, S. M. et al. Structural behavior of reinforced concrete incorporating glass waste as coarse aggregate. *J. Struct. Integr. Maintenance*. **8** (1), 59–66 (2023).
30. Pampana, L. D. et al. Evaluating the Mechanical Performance of Waste Glass Powder as a Fine Aggregate Substitute to Enhance Sustainability in Concrete Production. in IOP Conference Series: Earth and Environmental Science. IOP Publishing. (2023).
31. Yu, R. et al. Development of ultra-lightweight fibre reinforced concrete applying expanded waste glass. *J. Clean. Prod.* **112**, 690–701 (2016).
32. Jin, Z. et al. Mechanical properties and life cycle assessment (LCA) of waste glass reinforced concrete. *J. Building Eng.* **96**, 110643 (2024).
33. Rajagopalan, P. et al. Study of bond characteristics of reinforced waste glass aggregate concrete. in IOP Conference Series: Earth and Environmental Science. IOP Publishing. (2017).
34. Yassen, M. M., Hama, S. M. & Mahmoud, A. S. Shear behavior of reinforced concrete beams incorporating waste glass powder as partial replacement of cement. *Eur. J. Environ. Civil Eng.* **27** (5), 2194–2209 (2023).
35. Duxson, P. et al. The role of inorganic polymer technology in the development of 'green concrete'. *Cem. Concr. Res.* **37** (12), 1590–1597 (2007).
36. Yuan, X. et al. Integrated assessment of economic benefits and environmental impact in waste glass closed-loop recycling for promoting glass circularity. *J. Clean. Prod.* **444**, 141155 (2024).
37. Karalar, M. et al. Utilizing recycled glass powder in reinforced concrete beams: comparison of shear performance. *Sci. Rep.* **15** (1), 6919 (2025).
38. Aksoylu, C. et al. Experimental, theoretical and digital image correlation methods to assess bending performance of RC beams with recycled glass powder replacing cement. *Sci. Rep.* **15** (1), 25163 (2025).
39. Zeybek, O. et al. *Shear Performance in Reinforced Concrete Beams with Partial Aggregate Substitution Using Waste Glass: A Comparative Analysis Via Digital Imaging Processing and a Theoretical Approach* (ACS omega, 2024).
40. Çelik, A. İ. et al. Mechanical behavior of crushed waste glass as replacement of aggregates. *Materials* **15** (22), 8093 (2022).
41. Abdallah, S. & Fan, M. Characteristics of concrete with waste glass as fine aggregate replacement. *Int. J. Eng. Tech. Res.* **2** (6), 11–17 (2014).
42. West, G. *Alkali-aggregate Reaction in Concrete Roads and Bridges* (Thomas Telford, 1996).
43. Meyer, C. & Xi, Y. Use of recycled glass and fly Ash for precast concrete. *J. Mater. Civ. Eng.* **11**(2), 89–90 (1999).
44. Mirzahosseini, M. & Riding, K. A. Influence of different particle sizes on reactivity of finely ground glass as supplementary cementitious material (SCM). *Cem. Concr. Compos.* **56**, 95–105 (2015).
45. Terro, M. J. Properties of concrete made with recycled crushed glass at elevated temperatures. *Build. Environ.* **41** (5), 633–639 (2006).
46. Commitee, A. C. I. *State-of-the-art Report on alkali-aggregate Reactivity (221.1 R-98)* (American Concrete Institute, 1998).
47. 130, A. C. *ACI 130R-19 Report on the Role of Materials in Sustainable Concrete Construction* (American Concrete Institute, 2019).
48. Ispir, M., Ates, A. O. & Ilki, A. Low strength concrete: Stress-strain curve, modulus of elasticity and tensile strength. *Structures* **38**, 1615–1632 (2022).
49. Carrillo, J., Lozano, H. & Arteta, C. Mechanical properties of steel reinforcing bars for concrete structures in central Colombia. *J. Building Eng.* **33**, 101858 (2021).
50. Aci, C. *ACI 318 – 19: Building Code Requirements for Structural Concrete and Commentary* (American Concrete Institute, 2019).
51. Subramanian, N. *Design of Reinforced Concrete Structures* (oxford, 2013).
52. Najim, K. B. Determination and enhancement of mechanical and thermo-physical behaviour of crumb rubber-modified structural concrete. (2012).

Author contributions

Conceptualization, YOÖ, ÖZ and MK; methodology, YOÖ, ÖZ, MK and CA; data curation, YOÖ; investigation, YOÖ, BB, MK and ÖZ; validation, YOÖ, ÖZ, ES and OAU; visulation, BB, EA, AB, SS, ES, and OAU; Writing-original draft preparation, YOÖ, MK, CA, AB, SS, BB, ES, EA and OAU; writing-review and editing, YOÖ, MK, BB, ÖZ, CA, EA, AB, SS, ES, and OAU; funding acquisition, EA. All authors have read and agreed to the published version of the manuscript.

Funding

The authors are thankful for the financial support provided for this research by the Deanship of Scientific Research at King Khalid University, Abha, Saudi Arabia, through Large Groups RGP2/539/46.

Declarations

Competing interests

The authors declare no competing interests.

Additional information

Correspondence and requests for materials should be addressed to Y.O.Ö., A.N.B. or O.A.U.